© 2018. Published by The Company of Biologists Ltd | Development (2018) 145, dev169276. doi:10.1242/dev.169276

RESEARCH ARTICLE

A novel population of Hopx-dependent basal radial glial cells in the developing mouse neocortex

Samir Vaid[1], J. Gray Camp[2], Lena Hersemann[1], Christina Eugster Oegema[1], Anne-Kristin Heninger[1], Sylke Winkler[1], Holger Brandl[1], Mihail Sarov[1], Barbara Treutlein[2], Wieland B. Huttner[1,*] and Takashi Namba[1,*]

ABSTRACT

A specific subpopulation of neural progenitor cells, the basal radial glial cells (bRGCs) of the outer subventricular zone (OSVZ), are thought to have a key role in the evolutionary expansion of the mammalian neocortex. In the developing lissencephalic mouse neocortex, bRGCs exist at low abundance and show significant molecular differences from bRGCs in developing gyrencephalic species. Here, we demonstrate that the developing mouse medial neocortex (medNcx), in contrast to the canonically studied lateral neocortex (latNcx), exhibits an OSVZ and an abundance of bRGCs similar to that in developing gyrencephalic neocortex. Unlike bRGCs in developing mouse latNcx, the bRGCs in medNcx exhibit human bRGC-like gene expression, including expression of Hopx, a human bRGC marker. Disruption of Hopx expression in mouse embryonic medNcx and forced Hopx expression in mouse embryonic latNcx demonstrate that Hopx is required and sufficient, respectively, for bRGC abundance as found in the developing gyrencephalic neocortex. Taken together, our data identify a novel bRGC subpopulation in developing mouse medNcx that is highly related to bRGCs of developing gyrencephalic neocortex.

KEY WORDS: Basal radial glial cell, Development, Evolution, Hopx, Neocortex

INTRODUCTION

Neocortex expansion is one of the hallmarks of mammalian evolution (Rakic, 2009; Lui et al., 2011; Kaas, 2013; Sun and Hevner, 2014; Bae et al., 2015; Dehay et al., 2015; Lodato and Arlotta, 2015; Fernandez et al., 2016; Lein et al., 2017; Namba and Huttner, 2017; Sousa et al., 2017; Mitchell and Silver, 2018). This expansion involves an increase in the production of neurons from neural progenitor cells during cortical development. There are two principal classes of cortical progenitors (Götz and Huttner, 2005; Lui et al., 2011; Taverna et al., 2014; Dehay et al., 2015; Fernandez et al., 2016; Namba and Huttner, 2017): first, apical progenitors (APs), notably apical (or ventricular) radial glial cells (aRGCs), which contact the ventricle, are integrated into the apical adherens junction belt, and their nuclei reside in the ventricular zone (VZ) where they undergo mitosis at the apical surface; second, basal progenitors (BPs), specifically basal intermediate progenitors (bIPs) and basal (or outer) radial glial cells (bRGCs), which are delaminated from the ventricular surface and the apical adherens junction belt and the nuclei of which reside in the subventricular zone (SVZ) where they typically undergo mitosis. The main progeny of aRGCs are BPs, and the vast majority of the neurons generated in the developing neocortex originate from BPs (Lui et al., 2011; Dehay et al., 2015; Fernandez et al., 2016; Namba and Huttner, 2017).

In line with the latter statement, the evolutionary expansion of the neocortex has been linked to an increase in the proliferative capacity and abundance of BPs and, accordingly, in the thickness of the SVZ (Lui et al., 2011; Dehay et al., 2015; Fernandez et al., 2016; Namba and Huttner, 2017). In this context, a seminal finding was the identification and characterization of the outer SVZ (OSVZ) as the key germinal zone involved in neocortex expansion (Smart et al., 2002). Furthermore, the subsequent characterization of bRGCs (Fietz et al., 2010; Hansen et al., 2010; Reillo et al., 2011; Martinez-Cerdeno et al., 2012; Betizeau et al., 2013) provided additional insight, implicating this BP type, in particular, in cortical expansion (Lui et al., 2011; Stahl et al., 2013; Dehay et al., 2015; Fernandez et al., 2016; Namba and Huttner, 2017).

In addition to the differences in neocortex expansion among mammals, the neocortex exhibits a characteristic macroscopic feature, i.e. it is either smooth, referred to as lissencephalic, or folded, referred to as gyrencephalic (Rakic, 2009; Lui et al., 2011; Kaas, 2013; Sun and Hevner, 2014; Dehay et al., 2015; Striedter et al., 2015; Fernandez et al., 2016; Namba and Huttner, 2017). The degree of gyrencephaly varies considerably among mammals, ranging from a near-lissencephalic neocortex like that of the common marmoset to a highly folded neocortex like that of the dolphin (Lewitus et al., 2014; Striedter et al., 2015).

With regard to the specific BP type associated with lissencephaly versus gyrencephaly, the overwhelming majority of the BPs in the canonical developing lissencephalic mouse neocortex are bIPs, with only a minor proportion of bRGCs (Shitamukai et al., 2011; Wang et al., 2011; Wong et al., 2015) (low bRGC/BP proportion). In contrast, in developing gyrencephalic neocortex (such as human or rhesus monkey), bRGCs occur at high abundance (Fietz et al., 2010; Hansen et al., 2010; Reillo et al., 2011; Betizeau et al., 2013) (reviewed by Florio and Huttner, 2014; Sun and Hevner, 2014; Namba and Huttner, 2017) (high bRGC/BP proportion). Although several recent reports have shown that bRGCs exist, albeit at low abundance, in the developing mouse neocortex (Shitamukai et al., 2011; Wang et al., 2011; Wong et al., 2015), it should be emphasized that they do not exhibit a primate-like behavior unless subjected to genetic manipulation (Wong et al., 2015; Wang et al., 2016). Moreover, as shown for mouse, the bRGCs found in this lissencephalic developing neocortex exhibit a gene expression pattern that is distinct from that of the bRGCs in a developing gyrencephalic neocortex and more similar to that of bIPs (Florio et al., 2015). Specifically, mouse bRGCs express the canonical bIP

[1]Max Planck Institute of Molecular Cell Biology and Genetics, Pfotenhauerstraße 108, D-01307 Dresden, Germany. [2]Max Planck Institute for Evolutionary Anthropology, Deutscher Platz 6, D-04103 Leipzig, Germany.

*Authors for correspondence (huttner@mpi-cbg.de; namba@mpi-cbg.de)

W.B.H., 0000-0003-4143-7201; T.N., 0000-0003-4875-666X

Received 25 June 2018; Accepted 18 September 2018

Development (2018) 145, dev169276. doi:10.1242/dev.169276

marker Tbr2 (Englund et al., 2005) that is not expressed in the majority of human bRGCs (Florio et al., 2015). Conversely, markers of human bRGCs, such as HOPX (Pollen et al., 2015; Nowakowski et al., 2016; Thomsen et al., 2016), have not been found to be expressed in mouse bRGCs in the dorsolateral telencephalon during embryonic corticogenesis (Fietz et al., 2012; Florio et al., 2015), although Hopx has been reported to be strongly expressed in the dentate gyrus of adult mouse hippocampus (De Toni et al., 2008; Li et al., 2015). There, Hopx has been implicated in neural progenitor cell self-renewal (De Toni et al., 2008; Li et al., 2015).

In the present study, we have identified a region of the developing mouse neocortex – the medNcx – that exhibits features found in, but not necessarily restricted to, a developing gyrencephalic neocortex, i.e. abundant bRGCs and an OSVZ-like germinal zone. Furthermore, the expression of Hopx in the bRGCs of mouse medNcx has prompted us to perform functional studies, which demonstrate that Hopx is necessary and sufficient to achieve a bRGC abundance, as found in a developing gyrencephalic neocortex.

RESULTS

MedNcx of embryonic mouse exhibits a thick SVZ containing a high proportion of Pax6-positive cells

At any stage of mouse embryonic development, the latNcx contains only a low proportion of bRGCs among the BPs in the SVZ (Shitamukai et al., 2011; Wang et al., 2011; Wong et al., 2015). This is in contrast to developing neocortex of gyrencephalic mammals, which exhibits a high proportion of bRGCs among BPs (Fietz et al., 2010; Hansen et al., 2010; Reillo et al., 2011; Betizeau et al., 2013). We explored whether there is any region in developing mouse neocortex that may exhibit an SVZ resembling that typically found in developing gyrencephalic neocortex, with a distinct ISVZ and OSVZ, and a high proportion of bRGCs. To this end, we first examined the mouse embryonic day (E) 14.5-18.5 neocortical germinal zones for the expression and distribution of Pax6, a transcription factor marker of RGCs (Götz et al., 1998; Osumi et al., 2008).

Consistent with findings we previously obtained with embryonic mouse neocortex, notably at mid-neurogenesis (Arai et al., 2011), we observed that in mouse E14.5, E16.5 and E18.5 latNcx, Pax6 is expressed in the VZ but is downregulated in the SVZ, with only a low proportion of SVZ nuclei being strongly Pax6$^+$ (Fig. 1A,B,F,H, and data not shown). In contrast, in the mouse medNcx at E18.5, but not at E14.5 and E16.5, Pax6 expression was observed not only in essentially all VZ nuclei, but also in a high proportion of SVZ nuclei (Fig. 1A,C,F,H).

To obtain clues to the proliferative versus neurogenic potential of the Pax6$^+$ cells in the SVZ of mouse E18.5 medNcx, we examined the expression of Tbr2, a transcription factor characteristic of neuronal lineage-committed cortical progenitor cells (Englund et al., 2005) that in mouse embryonic latNcx is typically found in nuclei in the basal VZ and SVZ at mid-neurogenesis (Englund et al., 2005) and at E18.5 (Fig. 1A,B). Remarkably, although largely absent from the VZ of E18.5 medNcx, Tbr2 expression in the SVZ revealed two distinct subzones: one adjacent to the VZ in which the vast majority of nuclei were Tbr2+; and another more basally located one with a lower, yet still abundant, occurrence of Tbr2$^+$ nuclei (Fig. 1A,C).

This pattern of Pax6 and Tbr2 expression in the SVZ of mouse E18.5 medNcx (Fig. 1A,C), in contrast to mouse embryonic latNcx (Englund et al., 2005; Arai et al., 2011) (Fig. 1A,B), was reminiscent of that reported for the developing latNcx of three gyrencephalic species, i.e. ferret, macaque and human (Fietz et al., 2010; Hansen et al., 2010; Reillo et al., 2011; Betizeau et al., 2013). In these species, as first described for foetal monkey neocortex (Smart et al., 2002), a distinct ISVZ and OSVZ can be distinguished (Fietz et al., 2010; Hansen et al., 2010; Reillo et al., 2011; Betizeau et al., 2013). Specifically, the OSVZ/ISVZ ratio of Pax6$^+$ nuclei has been shown to be greater than that of Tbr2$^+$ nuclei (Fietz et al., 2010), as confirmed here for E36 ferret (Fig. 1D) and gestational week (GW) 15 human (Fig. 1E) latNcx. Although these stages of ferret and human cortical development are distinct from that of mouse at E18.5, the patterns of Pax6$^+$ and Tbr2$^+$ nuclei in the two SVZ subzones of mouse E18.5 medNcx (Fig. 1C) were reminiscent of those in E36 ferret and GW15 human ISVZ and OSVZ. We will therefore refer to the SVZ subzone in mouse E18.5 medNcx that is adjacent to the VZ as ISVZ, and to the more basally located one as OSVZ.

We next determined the proportion of Tbr2$^+$ nuclei in the SVZ of mouse E18.5 medNcx, as well as the distribution of Tbr2$^+$ nuclei along the radial axis of the medial cortical wall. Almost all Tbr2$^+$ nuclei (99.4±1.1%) were found to be also Pax6$^+$ at this developmental stage (Fig. 1C). We did not detect a significant difference between latNcx and medNcx in the proportion of the Pax6$^+$ nuclei that were also Tbr2$^+$ (50-60%, Fig. 1I). However, the distribution of Pax6$^+$Tbr2$^-$ versus Pax6$^+$Tbr2$^+$ nuclei along the radial axis of the medial cortical wall showed a striking difference. Whereas the occurrence of Pax6$^+$Tbr2$^-$ nuclei showed a first peak in the VZ and a second peak in the region of the OSVZ adjacent to the intermediate zone (IZ), the occurrence of Pax6$^+$Tbr2$^+$ nuclei peaked in the ISVZ and adjacent region of the OSVZ (Fig. 1G). Taken together, our data reveal the existence, in mouse E18.5 medNcx, of an ISVZ-like and an OSVZ-like layer containing both Pax6$^+$Tbr2$^-$ and Pax6$^+$Tbr2$^+$ cell subpopulations, suggesting that these layers constitute germinal zones harboring proliferative as well as neurogenic BPs.

The Pax6-positive cells in the SVZ of medNcx of embryonic mouse are cycling bRGCs

As BPs comprise bIPs and bRGCs, we sought to determine whether the Pax6$^+$ cells in the SVZ of mouse E18.5 medNcx include cycling bRGCs. To achieve this, we first performed immunohistochemistry for PCNA (Arai et al., 2011), a marker of cycling cells. This revealed that – in comparison with the latNcx – the much thicker SVZ of the E18.5 medNcx contained abundant PCNA$^+$ cells, both in the ISVZ and OSVZ (Fig. 2A,B). Specifically, for both Pax6$^+$Tbr2$^-$ and Pax6$^+$Tbr2$^+$ cells, ∼90% and 70% of the nuclei in the ISVZ and OSVZ, respectively, were PCNA$^+$ (Fig. 2C,D). These data indicate that the Pax6$^+$ cells in the SVZ of mouse E18.5 medNcx are indeed cycling.

A characteristic cell biological feature of bRGCs is that they retain a basal process and/or an apically directed process through M phase, which can be revealed, for example, by immunostaining for phosphorylated vimentin (pVim) (Fietz et al., 2010; Betizeau et al., 2013). We therefore used pVim immunohistochemistry to explore whether the cycling Pax6$^+$ cells in the SVZ of mouse E18.5 medNcx exhibited this feature. In addition, pVim immunohistochemistry provided information about the abundance and spatial distribution of mitotic cells in mouse E18.5 medNcx. When compared with the latNcx (Fig. 2E,H,I), the E18.5 medNcx, in line with its much thicker SVZ, showed a more basal relative distribution of mitotic cells (Fig. 2F,H) and contained, per area, a substantially greater number of basal mitotic cells (Fig. 2I) with a basal process (Fig. 2J). These basal pVim$^+$ cells typically expressed not only Pax6, as expected, but also the RGC marker Sox2 (see Fig. S2C). Moreover, more than half of the Pax6$^+$ basal mitotic cells exhibited a basal

Development (2018) 145, dev169276. doi:10.1242/dev.169276

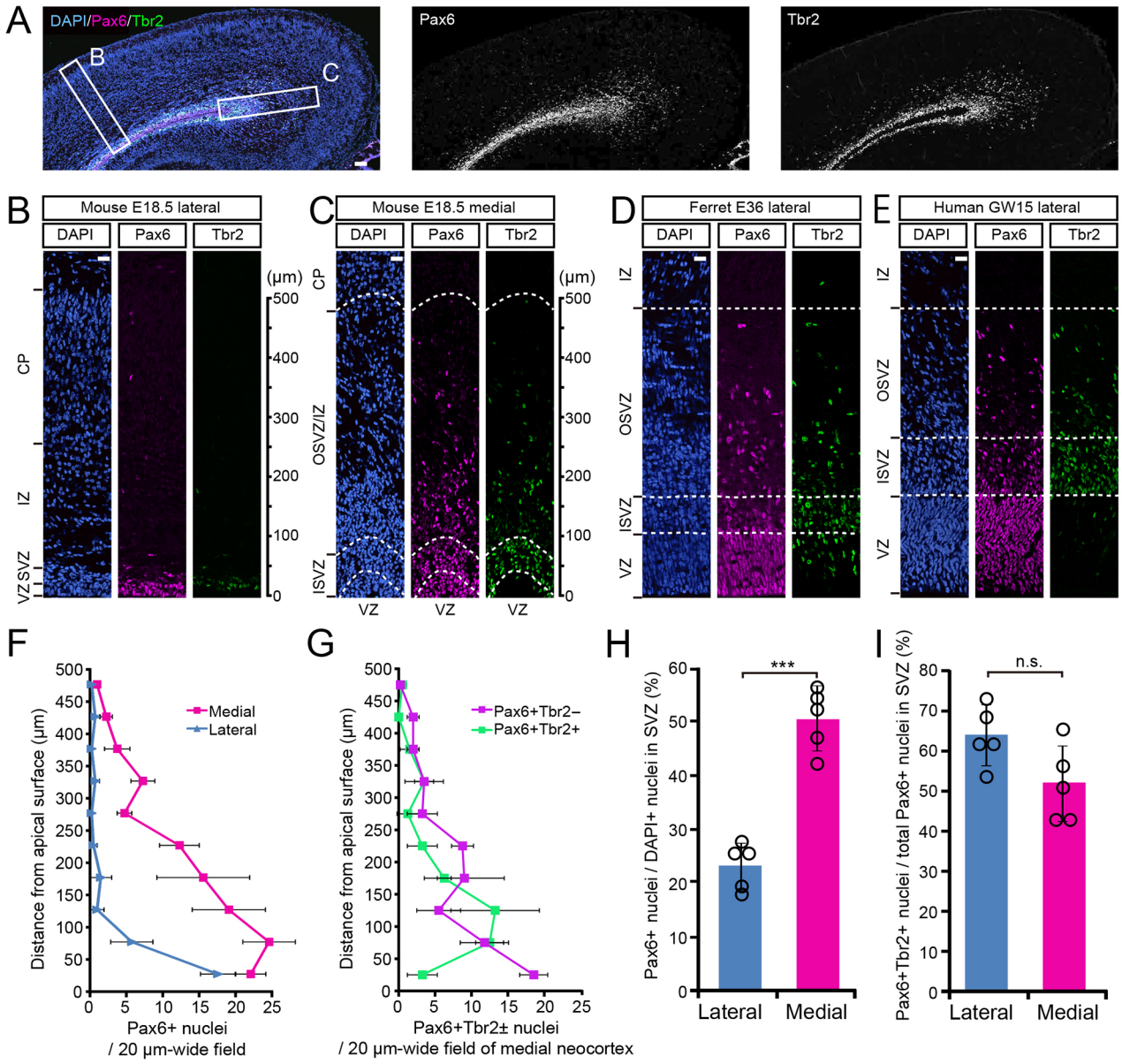

Fig. 1. Mouse E18.5 medNcx exhibits OSVZ-like features. (A-C) Mouse E18.5 caudal neocortex. Pax6 (magenta, white) and Tbr2 (green, white) double immunofluorescence, combined with DAPI staining (blue). (D,E) Ferret E36 latNcx (D) and human GW15 latNcx (E). Pax6 (magenta) and Tbr2 (green) double immunofluorescence, combined with DAPI staining (blue). (F) Quantification of the distribution of $Pax6^+$ nuclei along a 500 μm radial axis (divided into 10 bins) of the latNcx (blue) and medNcx (magenta). (G) Quantification of the distribution of $Pax6^+Tbr2^-$ (purple) and $Pax6^+Tbr2^+$ (green) nuclei along a 500 μm radial axis (divided into 10 bins) of the medNcx. (H,I) Quantification of the percentage of DAPI nuclei in the SVZ that are $Pax6^+$ (H) and of the percentage of $Pax6^+$ nuclei in the SVZ that are $Tbr2^+$ (I) in the latNcx (blue) and medNcx (magenta). (F-I) Error bars indicate s.d. ***P<0.001, n.s., not statistically significant. Student's t-test in H (n=5 embryos) and I (n=5 embryos). Open circles in H and I represent individual data points. (A-E) Images in B-E are single 0.6 μm optical sections; images in A are a 15 μm merged stack. Scale bars: 50 μm in A; 20 μm in B-E.

process (Fig. 2K,L; an example of such a cell, which lacks Tbr2 expression, is shown in Fig. 2G). Based on their morphology and marker expression, we conclude that about half of the mitotic cells in the SVZ of medNcx of E18.5 mouse are cycling bRGCs.

The progenitors in the SVZ of the medNcx of E18.5 mouse can give rise to neurons

We next investigated whether the bRGCs in medNcx of E18.5 mouse are neurogenic or gliogenic. To achieve this, we first analyzed the region of the cortical wall basal to the VZ for the expression of Olig2 (Fig. 3A,B), a marker of gliogenic precursors (Ono et al., 2009). We did not find a significant difference in the percentage of $Olig2^+$ cells between latNcx and medNcx (Fig. 3C). However, the percentage of the $Pax6^+Tbr2^-$ cells in medNcx [the majority of which are bRGCs (Fig. 2L)] that were $Olig2^+$ was significantly lower than that in latNcx (Fig. 3D), suggesting that bRGCs in the mouse E18.5 medNcx are less gliogenic than those in latNcx.

To directly determine the generation of neurons versus astrocytes that are found in medNcx when compared with the latNcx, we injected pregnant mice with 5-ethynyl-2-deoxyuridine (EdU) at E18.5. We then examined, at postnatal day (P) 10 (i.e. 11 days after EdU injection), the fate of the EdU^+ cells that were derived from the ones that had incorporated EdU and had reached the upper layers of the medNcx or latNcx, for the expression of NeuN, a neuron marker,

Development (2018) 145, dev169276. doi:10.1242/dev.169276

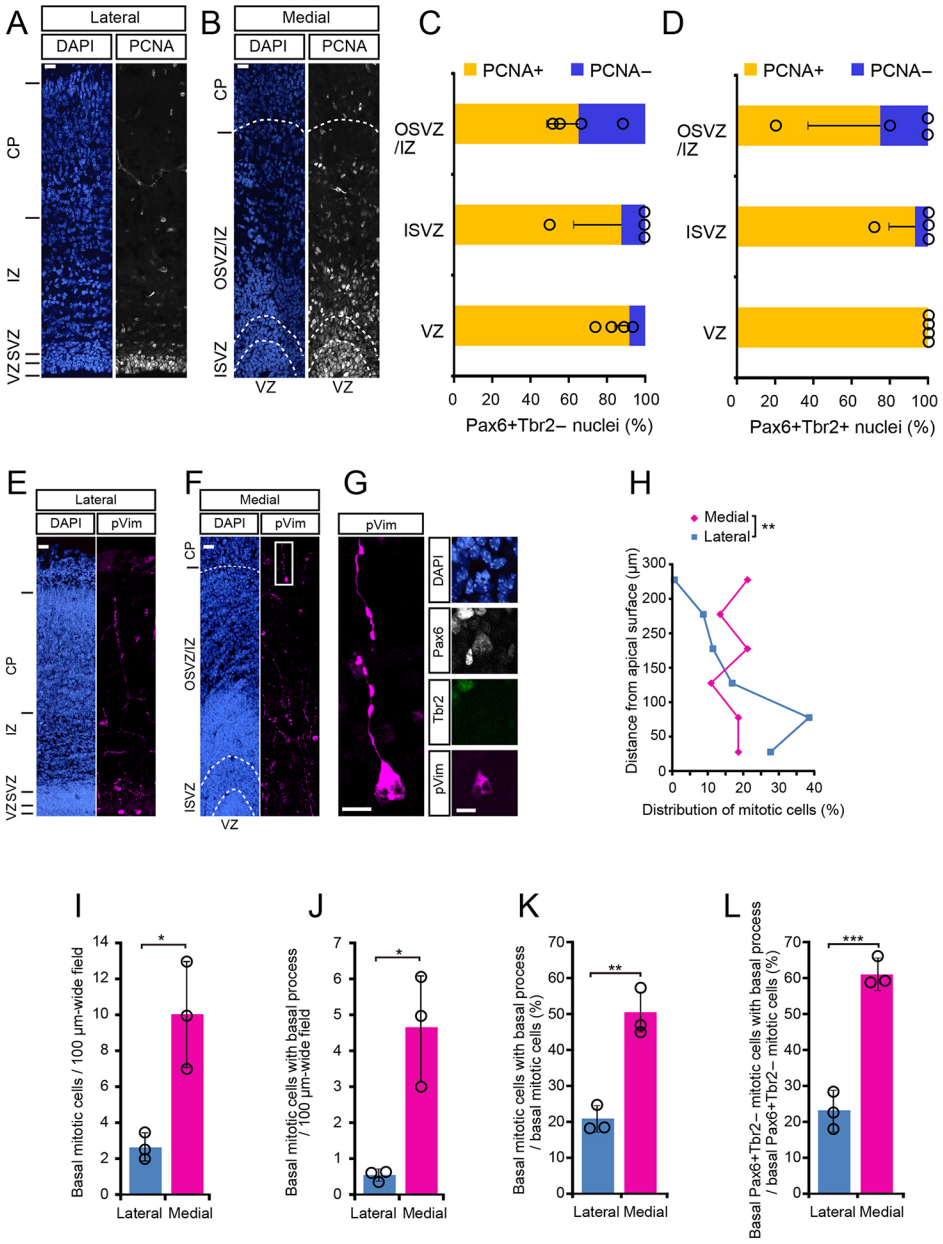

Fig. 2. The OSVZ of the mouse medNcx contains cycling bRGCs. (A,B) Mouse E18.5 latNcx (A) and medNcx (B). PCNA (white) immunofluorescence combined with DAPI staining (blue). (C,D) Quantification of the percentage of $Pax6^{+}Tbr2^{-}$ (C) and $Pax6^{+}Tbr2^{+}$ (D) nuclei that are $PCNA^{+}$ in the indicated zones of the mouse E18.5 medNcx. (E-G) Distribution of phosphorylated vimentin-positive ($pVim^{+}$) cells in mouse E18.5 latNcx (E) and medNcx (F). pVim (magenta) immunofluorescence, combined with DAPI staining (blue). White box in F indicates the area presented at higher magnification in G, showing a $pVim^{+}$ cell with a basal process. Right panels in G show Pax6 (white), Tbr2 (green) and pVim (magenta) triple-immunofluorescence, combined with DAPI staining (blue) in the area of the cell body of this cell. (H) Quantification of the distribution of mitotic cells (as revealed by pVim immunofluorescence) along a 300 µm radial axis (divided into six bins) of the latNcx (blue) and medNcx (magenta). (I) Quantification of basal (>30 µm from apical surface) mitotic ($pVim^{+}$) cells in the latNcx (blue) and medNcx (magenta). (J) Quantification of basal mitotic ($pVim^{+}$) cells with a basal process in latNcx (blue) and medNcx (magenta). (K) Quantification of percentage of basal mitotic cells ($pVim^{+}$) with a basal process in latNcx (blue) and medNcx (magenta). (L) Quantification of the percentage of basal $Pax6^{+}Tbr2^{-}$ mitotic ($pVim^{+}$) cells with a basal process in latNcx (blue) and medNcx (magenta). (C,D,H-L) Error bars indicate s.d.; $*P<0.05$; $**P<0.01$; $***P<0.001$. Mann-Whitney's *U*-test in H ($n=56$ cells in latNcx and 22 cells in medNcx); Student's *t*-test in I ($n=3$ embryos), K ($n=3$ embryos) and L ($n=3$ embryos); Welch's *t*-test in J ($n=3$ embryos). Open circles in bar graphs in C,D,I-L represent individual data points. (A,B,E-G) Images in A,B and right panels in G are single 0.4-0.6 µm optical sections; images in E,F and left panel in G are 10 µm merged stacks. Scale bars: 20 µm in A,B,E,F; 10 µm in G.

or S100β, an astrocyte marker (Fig. 3E,F,G). The percentage of the EdU^{+} cells that expressed S100β was slightly lower in the medNcx than in the latNcx, although this difference was not statistically significant (Fig. 3H). In contrast, compared with the latNcx, the percentage of the EdU^{+} cells that expressed NeuN was more than twofold greater in the upper layers of the medNcx (Fig. 3I). Of note, most of these E18.5-born neurons were located in the upper-most region of layer 2 (Fig. 3G). We conclude that the progenitors in mouse E18.5 medNcx exhibit a greater preference to generate neurons than those in E18.5 latNcx (for the analysis of EdU-labeled $NeuN^{+}$ neurons and $S100β^{+}$ astrocytes following an EdU pulse at P0, see Fig. S1).

The Hopx protein, a human bRGC marker, is specifically expressed in the germinal zones of the mouse E18.5 medNcx

Taken together, the results presented so far show that the mouse E18.5 medNcx, but not latNcx, SVZ exhibits a high abundance of bRGCs and an OSVZ-like layer. We therefore explored the possibility that the bRGCs in mouse E18.5 medNcx express genes characteristically expressed in bRGCs of developing human neocortex.

A search of the Allen Developing Mouse Brain Atlas, which covers ~2000 developmentally relevant genes (developingmouse.brain-map.org/), for genes expressed in a specific regional pattern at high intensity in E18.5 mouse forebrain yielded only one gene, the mRNA of which was specifically expressed in the medNcx: Hopx. Hopx is a homeodomain-only protein that does not bind to DNA and is the smallest member of the homeodomain-containing protein family (Mariotto et al., 2016). Although *Hopx* is expressed in regions of the mouse brain other than the neocortex (developingmouse.brain-map.org/), in human, HOPX has been identified as a bRGC marker in the developing neocortex at advanced stages of neurogenesis (Pollen et al., 2015; Thomsen et al., 2016). In light of these data, we searched previous transcriptome datasets of mouse E14.5 latNcx germinal zones (Fietz et al., 2012) and isolated progenitor subpopulations (Florio et al., 2015), and found Hopx mRNA expression in the VZ and aRGCs, but not in the SVZ and bRGCs,

Development (2018) 145, dev169276. doi:10.1242/dev.169276

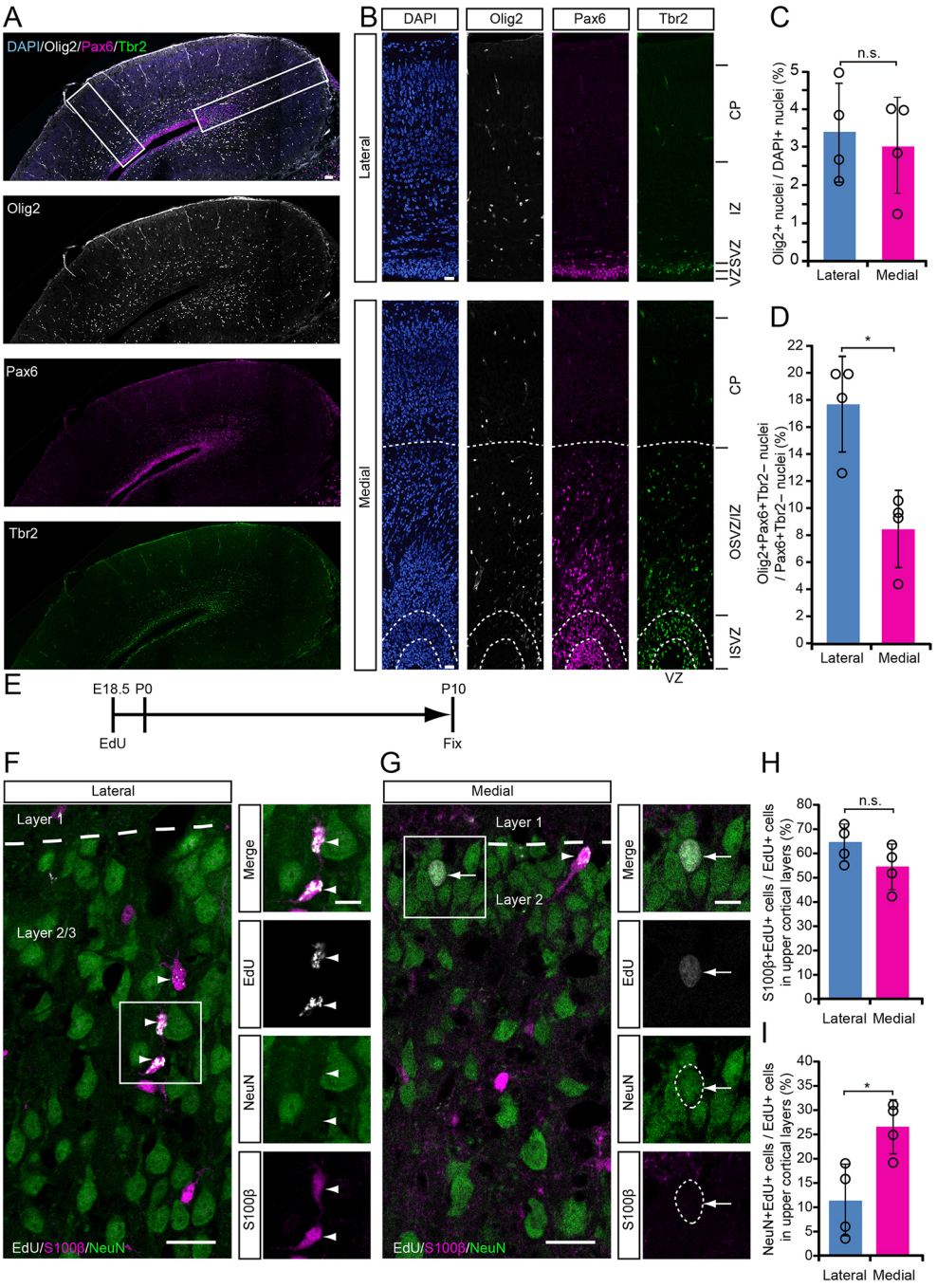

Fig. 3. Progenitor cells in mouse E18.5 medNcx contain a lesser proportion of gliogenic and a larger proportion of neurogenic precursors than latNcx. (A-D) A lesser proportion of the Pax6^{+}Tbr2^{-} cells in medNcx than latNcx expresses Olig2. (A,B) Olig2 (white), Pax6 (magenta) and Tbr2 (green) triple immunofluorescence, combined with DAPI staining (blue). White boxes in A indicate areas shown at higher magnification in B (top, latNcx; bottom, medNcx). (C) Quantification of the percentage of DAPI-positive nuclei that are Olig2^{+} in latNcx (blue) and medNcx (magenta) (20 µm wide field). (D) Quantification of the percentage of Pax6^{+}Tbr2^{-} cells that are Olig2^{+} in the latNcx (blue) and medNcx (magenta). (E-I) A larger proportion of the progenitor cells giving rise to the upper cortical layers are neurogenic in medNcx than in latNcx. Mice were labeled by an EdU pulse at E18.5 and analysed at P10 (see E). (F,G) EdU (white), NeuN (green) and S100β (magenta) triple immunofluorescence of cortical layers 2 and 3 [area within 200 µm of the boundary between layers 1 and 2 (dashed lines)] of P10 latNcx (F) and medNcx (G). White boxes indicate areas shown at higher magnification in the respective right panels. Arrowheads indicate S100β^{+}EdU^{+} cells; arrows and dashed circles indicate NeuN^{+}EdU^{+} cells. (H) Quantification of the percentage of EdU^{+} cells that are S100β^{+} in the lateral (blue) and medial (magenta) upper cortical layers. (I) Quantification of the percentage of EdU^{+} cells that are NeuN^{+} in the lateral (blue) and medial (magenta) upper cortical layers. (C,D,H,I) Error bars indicate s.d.; n.s., not statistically significant; *P<0.05. Student's t-test in C (n=4 embryos), D (n=4 embryos), H (n=4 mice) and I (n=4 mice). Open circles in C, D,H,I represent individual data points. (A, B,F,G) Images are single 0.4-0.6 µm optical sections. Scale bars: 50 µm in A; 20 µm in B and left panels in F,G; 10 µm in right panels in F,G.

of latNcx (data not shown), consistent with the absence of an OSVZ-like structure in this cortical region. However, given the presence of an OSVZ-like structure and of Hopx mRNA in the mouse E18.5 medNcx, we investigated whether the Hopx protein is expressed in this cortical region.

Consistent with previous Hopx mRNA *in situ* hybridisation data (Muhlfriedel et al., 2005, 2007), immunoreactivity for the Hopx protein was detected in the mouse E18.5 medNcx (Fig. 4A,C,F,G), but not latNcx (Fig. 4A,B,D,E), both in rostral (Fig. 4A,C) and caudal (Fig. 4A,F,G) areas. Importantly, the Hopx protein was detected not only in the VZ, but also in the ISVZ and OSVZ (Fig. 4G). This pattern of Hopx immunoreactivity was observed with both a rabbit polyclonal antibody (Fig. S2A-C) and a mouse monoclonal antibody (Fig. 4A,C,F,G). Although the latter antibody, in contrast to the rabbit polyclonal antibody, yielded nonspecific staining of blood vessels (Fig. 4A), it was nonetheless used in order to compare the immunostaining for Hopx with that of Pax6 (rabbit polyclonal antibody) and Tbr2 (chicken polyclonal antibody) (Fig. 4C,F,G). (For the analysis of Hopx protein expression during earlier stages of mouse embryonic development and during early postnatal stages, and to compare the similarity between Hopx expression in developing mouse medNcx and the human foetal neocortex, see Figs S2 and S3.)

Most proliferating bRGCs in E18.5 medNcx express the Hopx protein

The abundance of the Hopx^{+} cells in the E18.5 medNcx decreased from the VZ to the ISVZ to the OSVZ (Fig. 4H). Given the similar

Development (2018) 145, dev169276. doi:10.1242/dev.169276

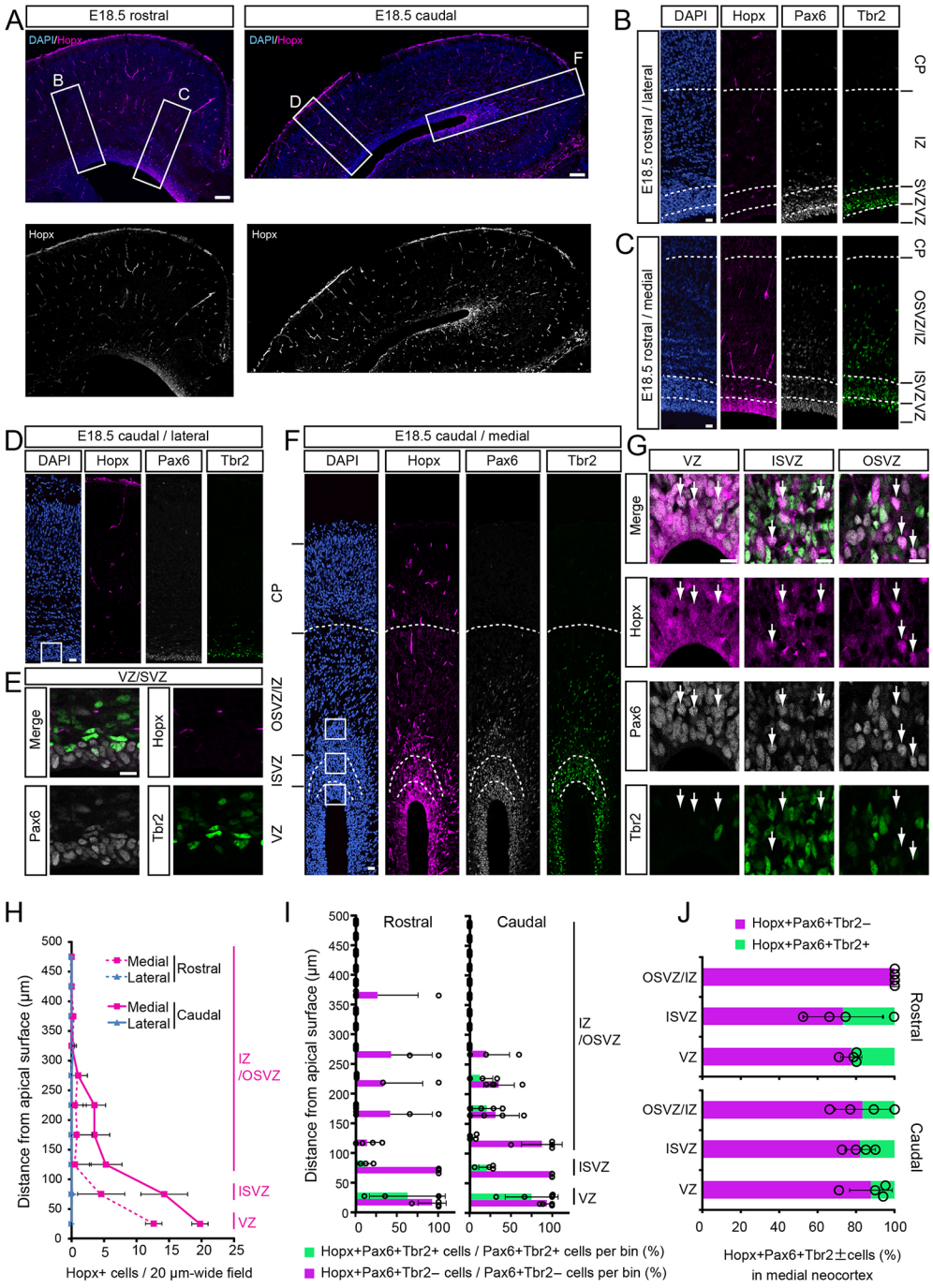

Fig. 4. Hopx protein is specifically expressed in the mouse E18.5 medNcx. (A) Hopx (magenta, white) immunofluorescence, combined with DAPI staining (blue, top images). (B,C) Hopx (magenta), Pax6 (white) and Tbr2 (green) triple immunofluorescence combined with DAPI staining (blue). (D-G) Hopx (magenta), Pax6 (white) and Tbr2 (green) triple immunofluorescence combined with DAPI staining (blue, D,F). White box in D indicates area shown at higher magnification in E; white boxes in F indicate VZ (apical box), ISVZ (middle box) and OSVZ (basal box) shown at higher magnification in G. Arrows in G indicate Hopx$^+$Pax6$^+$Tbr2$^-$ cells. (H) Quantification of the distribution of Hopx$^+$ cells along a 500 µm radial axis (divided into 10 bins) of rostral latNcx (dashed blue line), rostral medNcx (dashed magenta line), caudal latNcx (solid blue line) and caudal medNcx (solid magenta line). (I) Quantification of the percentage per bin of Pax6$^+$Tbr2$^-$ (magenta) and Pax6$^+$Tbr2$^+$ (green) cells that are Hopx$^+$ along a 500 µm radial axis (divided into 10 bins) of rostral (left plot) and caudal (right plot) medNcx (20 µm wide field). (J) Quantification of the percentages of Hopx$^+$ cells that are Pax6$^+$Tbr2$^-$ (green) and Pax6$^+$Tbr2$^+$ (magenta) in the indicated zones of rostral and caudal medNcx. (H-J) Error bars indicate s.d. Open circles in I,J represent individual data points (n=4 embryos). (A-G) Images in A are 11 µm merged stacks; images in B-G are single 0.6 µm optical sections. Scale bars: 50 µm in A; 20 µm in B-D,F and 10 µm in E,G.

pattern of abundance of the Pax6$^+$Tbr2$^-$ and Pax6$^+$Tbr2$^+$ cells in the E18.5 medNcx (Fig. 1), it was of interest to relate the Hopx expression to that of Pax6 and Tbr2 at the cellular level. Most of the Pax6$^+$Tbr2$^-$ cells in the VZ, ISVZ and apical-most region of the OSVZ were found to be Hopx$^+$, whereas only Pax6$^+$Tbr2$^+$ cells in the VZ showed Hopx immunoreactivity in the majority of cases (Fig. 4I). With regard to the bRGCs in the E18.5 medNcx, these data are consistent with the notion that Hopx expression occurs preferentially in proliferating bRGCs. In line with this notion, all Hopx$^+$ cells in the E18.5 medNcx germinal zones were Pax6$^+$ (Fig. 4J), and the vast majority of these Hopx$^+$ cells were Tbr2$^-$ (Fig. 4J) and Sox2$^+$ (Fig. S2E). Moreover, >80% of the basal mitoses in the E18.5 medNcx, as identified by pVim immunofluorescence, were Hopx$^+$ (Fig. S2D).

Taken together, these results show that, in contrast to the latNcx of the embryonic mouse, the mouse E18.5 medNcx exhibits key features also observed in the development of an expanded neocortex, as characterized in foetal human (Fietz et al., 2010; Hansen et al., 2010; Pollen et al., 2015; Nowakowski et al., 2016; Thomsen et al., 2016), foetal macaque (Smart et al., 2002; Betizeau et al., 2013) and embryonic ferret (Fietz et al., 2010; Reillo et al., 2011) (Fig. S2F) neocortex. These features notably include the existence of an OSVZ that contains proliferating Pax6$^+$ bRGCs extending a basal process and expressing the Hopx protein, a bRGC marker in the OSVZ at advanced stages of foetal human neocortical neurogenesis (Pollen et al., 2015; Nowakowski et al., 2016; Thomsen et al., 2016).

Development (2018) 145, dev169276. doi:10.1242/dev.169276

The bRGCs in embryonic mouse medNcx exhibit a human bRGC-like gene expression signature

To directly analyze whether the bRGCs in the embryonic mouse medNcx are distinct from the bRGCs in the embryonic mouse latNcx and, perhaps, are more related to the bRGCs in foetal human neocortex than the mouse lateral bRGCs, we took advantage of population-level RNA-sequencing of bRGCs isolated from E18.5 mouse medNcx. We first compared the gene expression of these bRGCs with that of various cortical progenitor populations previously isolated from E14.5 mouse latNcx (Florio et al., 2015). Using principal component analysis (PCA), we found that mouse medial bRGCs emerge as a distinct progenitor population that can be clearly distinguished from mouse lateral bRGCs, aRGCs and bIPs (Fig. 5A). We extended this analysis by performing PCA of mouse medial bRGCs and all cell populations previously isolated from embryonic mouse and foetal human neocortex (Florio et al., 2015), which, in addition to the cortical progenitor populations already analyzed (Fig. 5A), included *Tis21*-GFP-negative and -positive mouse lateral aRGCs, mouse neurons, GW15 human aRGCs, human bRGCs and a fraction enriched in human neurons (see Fig. S4).

To examine whether the mouse medial bRGCs exhibit human bRGC-like gene expression, we next analyzed and compared the expression levels of the previously identified 64 human bRGC-enriched genes (Pollen et al., 2015) or their mouse orthologs among the bRGCs isolated from E14.5 latNcx (Florio et al., 2015), E18.5 medNcx (present study) and human GW15 neocortex (Florio et al., 2015). As shown in Fig. 5B, a greater *Hopx* mRNA level was detected in the mouse medial bRGCs than the mouse lateral bRGCs, consistent with the present immunohistochemical results (Fig. S2A). We further found that for the overwhelming majority of the 64 human bRGC-enriched genes or their respective mouse orthologs, the expression levels in the mouse medial bRGCs were higher than in the mouse lateral bRGCs, and in many cases (e.g. *Gfap*, *Dio2*, *Bmp7*, *Fabp7*, *Ptprz1*, *Tnc*, *Veph1* and *Etv1*) approached or even exceeded those in the human bRGCs

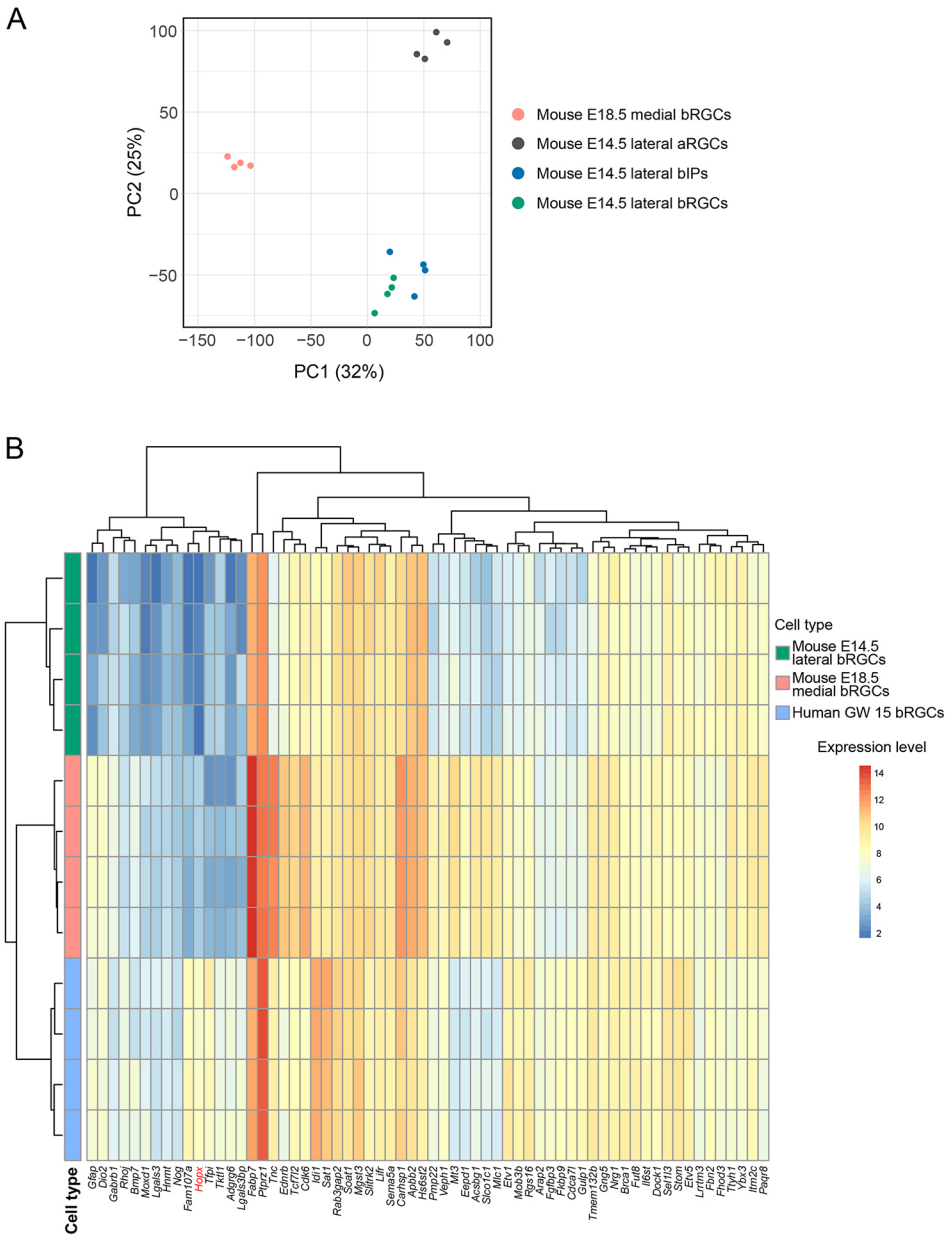

Fig. 5. bRGCs in mouse E18.5 medNcx exhibit a gene expression distinct from aRGCs, bRGCs and bIPs in mouse E14.5 latNcx, and express a human bRGC-like gene signature. Comparative analysis of RNA-seq data of: (1) bRGCs isolated from mouse E18.5 medNcx (this study; A,B); (2) cortical progenitor populations isolated from mouse E14.5 latNcx (Florio et al., 2015; GEO accession number GSE65000; A,B); and (3) bRGCs isolated from human GW 15 neocortex [(Florio et al., 2015), GSE65000; B]. (A) Principal component analysis of rlog-transformed counts. First and second principal component (PC1 and PC2) of mouse cortical progenitor samples (four replicates per indicated mouse cortical progenitor type, colored dots) are shown along with the proportion of variance explained. (B) Clustered heatmap of mouse medial (pink), mouse lateral (green) and human (blue) bRGC populations based on rlog-transformed counts of the 64 human bRGC-enriched genes and their mouse orthologs. Horizontal rows (replicates of each of the three bRGC populations) and vertical columns (genes) were hierarchically clustered using complete linkage and Euclidian distance.

Development (2018) 145, dev169276. doi:10.1242/dev.169276

(Fig. 5B). In fact, hierarchical clustering indicated that the mouse medial bRGCs were more closely related to human bRGCs than the mouse lateral bRGCs. These results indicate that the mouse medial bRGCs exhibit a human bRGC-like gene expression signature. These data were complemented by unbiased single-cell transcriptomics (see Fig. S5) and by an analysis of the expression levels of the orthologs of the 64 human bRGC-enriched genes (Pollen et al., 2015) in the OSVZ of a prospective gyrus versus a prospective sulcus of developing ferret neocortex (De Juan Romero et al., 2015) (see Fig. S6).

Disruption of Hopx expression in the embryonic mouse medNcx reduces the abundance of bRGCs

We investigated a potential functional role of Hopx in the bRGCs of the mouse embryonic medNcx SVZ, using CRISPR/Cas9-mediated gene disruption (for details, see Fig. S7). Analysis of the proportion of $Hopx^+$ cells among the RFP^+ cells in the VZ and SVZ revealed that CRISPR/Cas9-mediated disruption of *Hopx* gene expression almost completely abolished the occurrence of $Hopx^+$ cells among the progeny of the targeted cells found in the VZ, and completely did so for the SVZ (Fig. 6A,B).

Such a disruption of Hopx expression in the embryonic mouse medNcx did not affect the abundance of the $Sox2^+Tbr2^+RFP^+$ cells and the $Sox2^+Tbr2^-RFP^+$ cells in the VZ but reduced the abundance of the $Sox2^+Tbr2^-RFP^+$ cells in the SVZ about twofold (Fig. 6C-G). This decrease in $Sox2^+Tbr2^-RFP^+$ cells in the SVZ was accompanied by a significant increase in the number of $Sox2^-Tbr2^+RFP^+$ cells. The decrease in the $Sox2^+Tbr2^-RFP^+$ SVZ cells was observed irrespective of whether the quantification was performed per total RFP^+ SVZ cells (Fig. 6F) or per SVZ area (Fig. 6G), eliminating the possibility that it reflected differences in the efficiency of *in utero* electroporation. Furthermore, disruption of Hopx expression markedly reduced the abundance of basal $Sox2^+RFP^+$ cells in mitosis, as revealed by pVim immunofluorescene (Fig. 6H-J), and of total BPs in mitosis, as revealed by immunofluorescence for phosphorylated histone H3 (PH3) (Fig. S7G-I). The proportion of the $Sox2^+RFP^+$ mitotic BPs that exhibited a basal process at mitosis did not differ between control and Hopx gene disruption (Fig. 6K). These results demonstrate that Hopx is required to maintain the level of $Sox2^+$ progenitors in the SVZ of embryonic mouse medNcx, with the majority of these progenitors presumably being bRGCs (see Fig. 2L, Fig. 4J). (For the analysis of the potential consequence for neurogenesis of the reduced abundance of $Sox2^+$ SVZ progenitors in embryonic mouse medNcx upon disruption of Hopx expression, see Fig. S8.)

Forced expression of Hopx in the embryonic mouse latNcx increases the abundance of bRGCs

Only a minor proportion of the progenitors residing in the SVZ of mouse E18.5 latNcx are bRGCs (Shitamukai et al., 2011; Wang et al., 2011; Wong et al., 2015) (Fig. 1B,F,H, Fig. 2K,L). As the expression of the Hopx protein in the latNcx decreases from E15.5 to E18.5 and is lacking at the latter stage (Fig. S2A), and given the essential role of Hopx in maintaining the level of bRGCs in the SVZ of embryonic mouse medNcx (Fig. 6F,G,J), we explored whether forced Hopx expression in the embryonic mouse latNcx would increase bRGC abundance.

To achieve this, we expressed Hopx under the control of a constitutive promoter, along with a GFP reporter, in the latNcx by *in utero* electroporation at E15.5, and analyzed the abundance and distribution of progenitor cells at E18.5 (Fig. 7A,B). The presence of the Hopx protein in the progeny of the electroporated cells was confirmed by immunofluorescence (Fig. S9). Analysis of the progeny of the electroporated cells by immunofluorescence for pVim showed that this forced Hopx expression did not significantly alter the level of APs undergoing mitosis (Fig. 7C). In contrast, forced Hopx expression tripled the level of mitotic BPs in the latNcx that were derived from the electroporated cells (Fig. 7D). This increase in BPs included an increase in basally located $Pax6^+$ cells, which were observed not only in the SVZ but, notably, also in the IZ (Fig. 7E). Moreover, the proportion of the $Pax6^+GFP^+$ BPs that exhibited a basal process at mitosis (Fig. 7H) was threefold greater upon forced Hopx expression than in the control (Fig. 7I). When the GFP^+ cells in the VZ were analyzed for Tbr2 expression, the proportion of the $Pax6^+Tbr2^-$ cells and the $Pax6^+Tbr2^+$ cells was not changed upon forced Hopx expression (Fig. 7F). In contrast, analysis of the GFP^+ cells in the SVZ-IZ revealed: (1) a marked increase in the proportion of $Pax6^+Tbr2^-$ cells; (2) an increase (albeit not statistically significant) in the proportion of $Pax6^+Tbr2^+$ cells; and (3) no change in the proportion of $Pax6^-Tbr2^+$ cells (Fig. 7G). Together, these results demonstrate that forced Hopx expression in the embryonic mouse latNcx does not affect AP abundance but is sufficient to increase the abundance of BPs and promotes the generation of bRGCs among these BPs (please see Discussion for the issue of cortical folding). (For the analysis of the potential effects on neurogenesis of the increased bRGC abundance in the embryonic mouse latNcx caused upon forced Hopx expression, see Fig. S10.)

DISCUSSION

The present study provides two advances with regard to our insight into the development of the cerebral cortex. First, we identify a region in the embryonic mouse neocortex – the medNcx – that exhibits a bRGC/BP proportion as high as that typically found in a developing gyrencephalic neocortex. Second, we demonstrate that the mouse ortholog of a marker of human bRGCs, Hopx, is necessary and sufficient for such a high bRGC/BP proportion. These findings may have implications for the evolution of the lissencephalic mouse neocortex.

Hopx – a determinant of bRGC abundance

Our data indicate that Hopx is necessary and sufficient to achieve an abundance of bRGCs that is essentially as high as that typically observed in a developing gyrencephalic neocortex (e.g. human; Fietz et al., 2010). Specifically, CRISPR/Cas9-mediated disruption of Hopx expression in the embryonic mouse medNcx reduced the relative abundance of bRGCs from ~50% of all BPs (see Fig. 2K) to a level essentially as low as that seen in embryonic mouse latNcx [at most 20% of all BPs (Shitamukai et al., 2011; Wang et al., 2011; Wong et al., 2015); Fig. 2K] (Fig. 6F,G,J). Conversely, forced Hopx expression in the embryonic mouse latNcx increased the relative abundance of bRGCs to the level seen in the mouse E18.5 medNcx (Fig. 7D-F). The present data therefore establish Hopx as a key determinant of bRGC abundance in the developing neocortex.

Further studies will be required to determine whether an increase in bRGC abundance due to Hopx expression can promote neocortical folding, as has been observed previously upon forced expression in embryonic mouse neocortex of ARHGAP11B (Florio et al., 2015) and sonic hedgehog (Wang et al., 2016), or upon knockdown of Trnp1 (Stahl et al., 2013). On the one hand, we did not observe neocortical folding upon forced Hopx expression in embryonic mouse latNcx by P1 (Fig. S10A and data not shown). Moreover, we found abundant $Hopx^+$ cells in the OSVZ of the latNcx of embryonic marmoset (data not shown), a near-lissencephalic primate. On the other hand, we noticed upon data

Development (2018) 145, dev169276. doi:10.1242/dev.169276

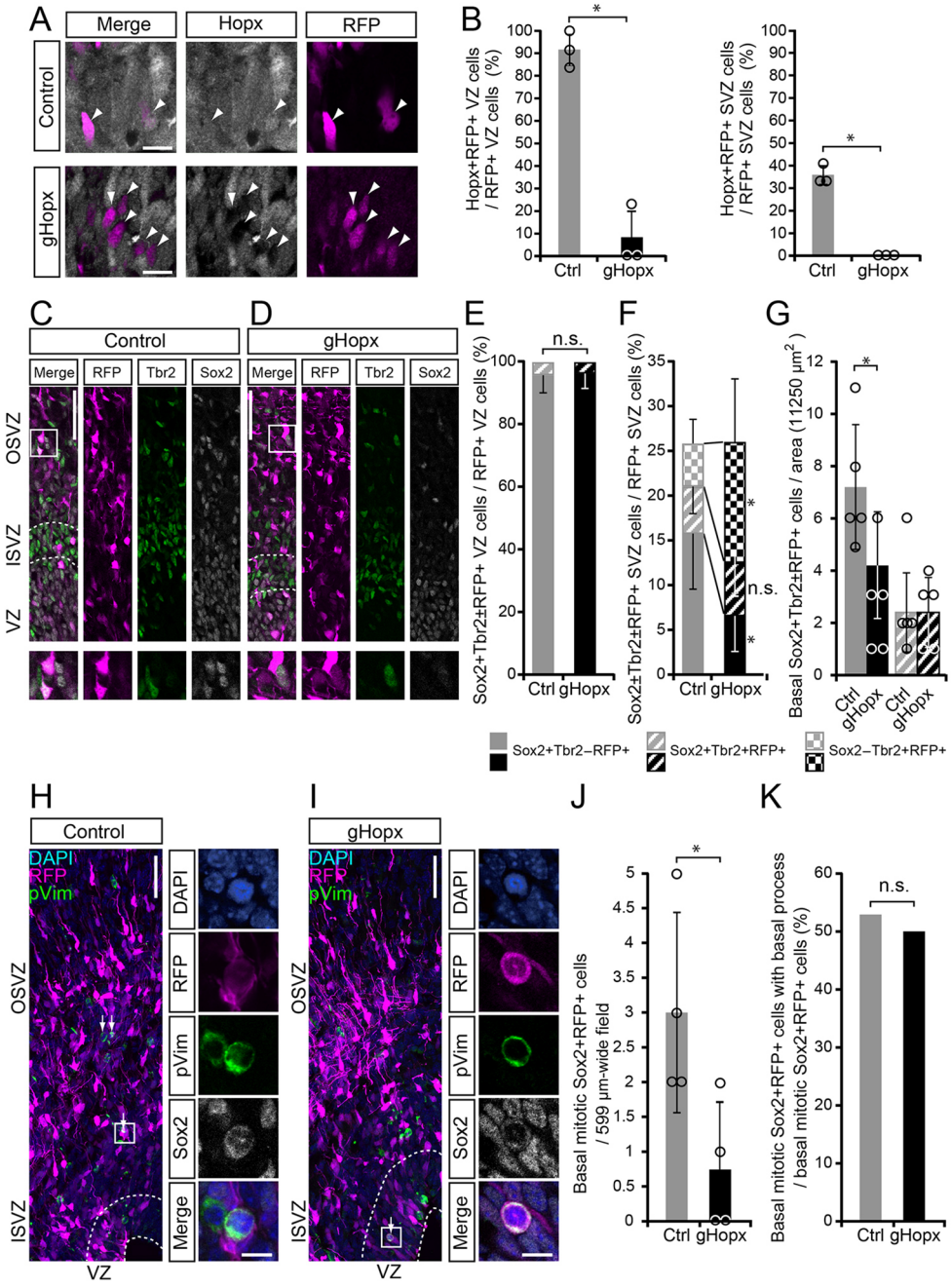

Fig. 6. CRISPR/Cas9-mediated disruption of Hopx expression in embryonic mouse medNcx decreases cycling bRGCs. MedNcx of mouse E15.5 embryos was *in utero* electroporated with either a plasmid encoding Cas9_T2A_PaprikaRFP and a gRNA targeting *LacZ* (control, Ctrl), or with a mixture of two plasmids, each encoding Cas9_T2A_PaprikaRFP and one of the two gRNAs targeting Hopx (gHopx, either gRNA #10 or gRNA #13, see Fig. S7), all under constitutive promoters, followed by analysis at E18.5. (A) RFP (magenta) and Hopx (white) double immunofluorescence of the VZ. Arrowheads indicate RFP$^+$ cells; note the presence of Hopx immunoreactivity in the control RFP$^+$ cells (top) and its absence in the RFP$^+$ cells upon gHopx electroporation (bottom). (B) Quantification of the proportion of RFP$^+$ cells in the VZ (left) and SVZ (right) that are Hopx$^+$ upon control (gray) and gHopx (black) electroporation. (C,D) RFP (magenta), Tbr2 (green) and Sox2 (white) triple immunofluorescence, upon control (C) and gHopx (D) electroporation. White boxes in left panels indicate areas shown at higher magnification in the respective bottom panels. (E) Quantification of percentage of RFP$^+$ cells in VZ that are Sox2$^+$Tbr2$^-$ (solid) and Sox2$^+$Tbr2$^+$ (stripe) upon control (gray) and gHopx (black) electroporation. (F) Quantification of percentage of RFP$^+$ cells in SVZ that are Sox2$^+$Tbr2$^-$ (solid), Sox2$^+$Tbr2$^+$ (stripe) and Sox2$^-$Tbr2$^+$ (checked) upon control (gray) and gHopx (black) electroporation. (G) Quantification of basal RFP$^+$ cells in ISVZ plus OSVZ (11,250 µm^2 area) that are Sox2$^+$Tbr2$^-$ (solid) and Sox2$^+$Tbr2$^+$ (stripe) upon control (gray) and gHopx (black) electroporation. (H,I) RFP (magenta), pVim (green) and Sox2 (white) triple immunofluorescence, combined with DAPI staining (blue), upon control (H) and gHopx (I) electroporation. White boxes in left panels indicate areas shown at higher magnification in the respective right panels. Arrows indicate basal RFP$^+$ cells in mitosis, as revealed by pVim immunofluorescence. (J) Quantification of basal Sox2$^+$pVim$^+$RFP$^+$ cells upon control (gray) and gHopx (black) electroporation. (K) Quantification of percentage of basal Sox2$^+$pVim$^+$RFP$^+$ cells that retain a basal process upon control (gray) and gHopx (black) electroporation. (B,E-G,J) Error bars indicate s.d.; n.s., not statistically significant; *P<0.05. Mann-Whitney's U-test in B (n=3 embryos), J (n=4 embryos) and K (n=17 cells for control, 20 cells for gHopx); Student's t-test in E (n=4 embryos), F (n=4 embryos) and G (n=4 embryos). Open circles in bar graphs in B,G,J represent individual data points. (A,C,D,H,I) Images in A,C,D and in right panels in H,I are single 0.6 µm optical sections; images in left panels in H,I are 6 µm merged stacks. Scale bars: 50 µm in C,D and left panels in H,I; 10 µm in A and right panels in H,I.

Development (2018) 145, dev169276. doi:10.1242/dev.169276

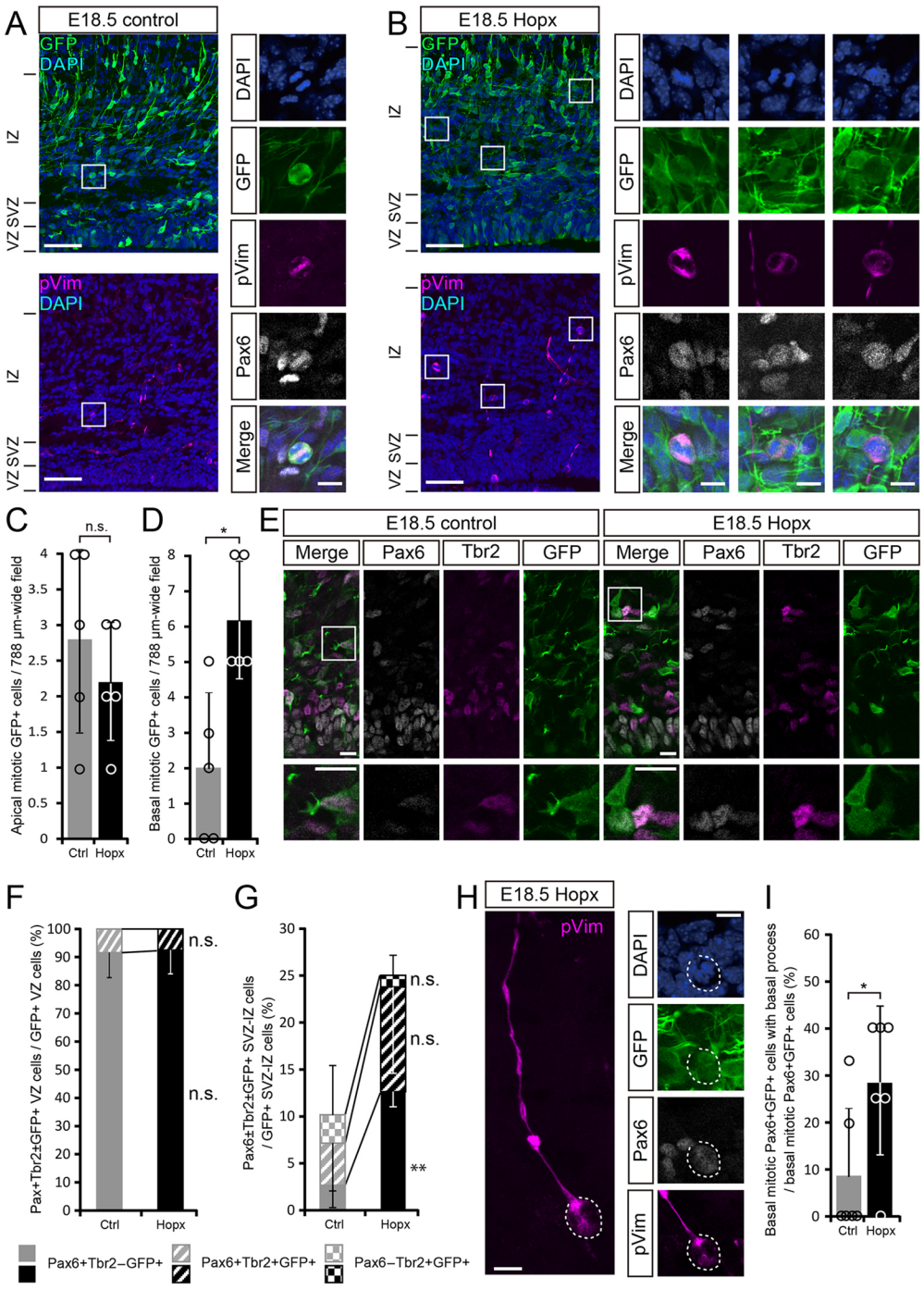

Fig. 7. Forced Hopx expression in embryonic mouse latNcx increases bRGCs. LatNcx of mouse E15.5 embryos was *in utero* co-electroporated with a plasmid encoding GFP together with either an empty vector (control, Ctrl) or a Hopx expression plasmid (Hopx) under constitutive promoters, followed by analysis at E18.5. (A,B) GFP (green), pVim (magenta) and Pax6 (white) triple immunofluorescence, combined with DAPI staining (blue), upon control (A) and forced Hopx expression (B). White boxes in left panels indicate areas shown at higher magnification in the respective right panels. (C,D) Quantification of apical (C) and basal (D) GFP$^+$ cells in mitosis (as revealed by pVim immunofluorescence) in control (gray) and upon forced Hopx expression (black). (E) GFP (green), Tbr2 (magenta) and Pax6 (white) triple immunofluorescence in control and upon forced Hopx expression. White boxes in left panels indicate areas shown at higher magnification in the respective bottom panels. (F) Quantification of percentage of GFP$^+$ cells in VZ that are Pax6$^+$Tbr2$^-$ (solid) and Pax6$^+$Tbr2$^+$ (stripe) in control (gray) and upon forced Hopx expression (black). (G) Quantification of percentage of GFP$^+$ cells in a region spanning the basal part of the SVZ and the adjacent part of the IZ (100 µm×100 µm field with its basal boundary 200 µm away from the apical surface) that are Pax6$^+$Tbr2$^-$ (solid), Pax6$^+$Tbr2$^+$ (stripe) and Pax6$^-$Tbr2$^+$ (checked) in control (gray) and upon forced Hopx expression (black). (H) Example of a bRGC (Pax6$^+$, white) with basal process in mitosis (DAPI, blue; pVim$^+$, magenta) upon forced Hopx expression (GFP$^+$); dashed circles indicate the cell body. (I) Quantification of percentage of basal Pax6$^+$GFP$^+$ cells in mitosis (pVim$^+$) that retain a basal process in control (gray) and upon forced Hopx expression (black). (C,D,F,G,I) Error bars indicate s.d.; n.s., not statistically significant; *P<0.05; **P<0.01. Student's t-test in C (n=5 embryos), F (n=3 embryos) and G (n=3 embryos); Mann-Whitney's U-test in D (n=5 embryos) and I (n=6 embryos). Open circles in C,D represent individual data points. (A,B,E,H) Images in left panels in A,B,H are 5-6 µm merged stacks; images in right panels in A,B,H and in E are single 0.6 µm optical sections. Scale bars: 50 µm in A,B (left panels); 10 µm in A,B (right panels) and E,H.

Development (2018) 145, dev169276. doi:10.1242/dev.169276

mining of the genes differentially expressed in the developing neocortex of the ferret (De Juan Romero et al., 2015), a gyrencephalic carnivore, that *Hopx* expression is higher in the OSVZ of a prospective gyrus than a prospective sulcus (Fig. S6), consistent with a greater bRGC abundance in the former (Reillo et al., 2011; Borrell and Götz, 2014). Our data therefore suggest that the primary function of Hopx is related to bRGC abundance, but do not exclude the possibility that an increased bRGC abundance due to Hopx expression, in concert with the effects of other factors, may promote neocortical folding.

bRGC abundance is determined by two principal processes: (1) the production of bRGCs from aRGCs; and (2) the self-expansion of bRGCs by symmetric proliferative divisions (Lui et al., 2011; Dehay et al., 2015; Fernandez et al., 2016; Namba and Huttner, 2017). In the developing ferret neocortex, bRGC self-expansion has been shown to largely occur after a defined time window of bRGC production from aRGCs (Martinez-Martinez et al., 2016). How, then, can the presence of Hopx protein in both aRGCs and bRGCs of mouse E18.5 medNcx be interpreted? First, the presence of Hopx in the medial aRGCs may be indicative of a role in bRGC production, rather than in aRGC self-expansion. Support for the latter scenario being unlikely is provided by our findings that disruption of Hopx expression in the medial aRGCs did not decrease their pool size (Fig. 6E), and forced Hopx expression in the lateral aRGCs did not increase their pool size (Fig. 7C). Second, the presence of Hopx in the medial bRGCs likely suggests that it promotes bRGC self-expansion. The marked decrease in bRGC abundance (Fig. 6F,G,J), without a concomitant increase in aRGC abundance (Fig. 6E), upon disruption of Hopx expression in the mouse embryonic medNcx supports this view.

The embryonic mouse medNcx – a relict of an ancestral gyrencephalic developing cerebral cortex?

The present finding that the embryonic mouse medNcx, in contrast to the latNcx, exhibits an OSVZ-like germinal zone with abundant bRGCs may have implications for the evolution of the lissencephalic mouse neocortex. It has previously been proposed that all mammals evolved from a common gyrencephalic ancestor (O'Leary et al., 2013; Lewitus et al., 2014) and that the mouse lissencephaly is secondary in nature, reflecting phyletic dwarfing (Kelava et al., 2013; Lewitus et al., 2014). If so, one would expect to find any relicts of this gyrencephalic ancestor in the developing medNcx rather than latNcx, as the former constitutes an evolutionarily older part of the neocortex than the latter (Sanides, 1969). The OSVZ-like germinal zone with abundant bRGCs, which is a typical feature of a developing gyrencephalic neocortex and that we observed in the embryonic mouse medNcx, would be consistent with this scenario. This notion is not contradicted by the previous finding that the embryonic neocortex of the common marmoset also exhibits an OSVZ-like germinal zone with abundant bRGCs, as the marmoset has also been proposed to have evolved from a gyrencephalic ancestor (Kelava et al., 2013); OSVZ and abundant bRGCs may also be relicts of this ancestor.

In this context, two previous observations should be noted. First, the gyrification of the mouse neocortex that could be induced by an activation of the sonic hedgehog signaling pathway during embryonic corticogenesis was found to primarily take place in the cingulate cortex (Wang et al., 2016), which belongs to the medNcx. As the specific approach taken by the authors resulted in activation of the sonic hedgehog signaling pathway not only in the embryonic mouse medNcx but also the adjacent latNcx (Wang et al., 2016), this finding suggests that the medNcx of embryonic mouse, specifically, may be particularly 'gyrification-prone', as would be expected if it retains features of an ancestral gyrencephalic neocortex.

Second, gyrification is a characteristic feature of the hippocampus (i.e. the dentate gyrus) in most mammals but not in birds and reptiles. In fact, there may be a parallel with regard to the evolution of cortical folding between the mammalian dendate gyrus, which arises from the medial cerebral cortex, and the mouse medNcx, which appears to retain ancestral gyrencephalic features (Hevner, 2016). It is therefore interesting to note that the dentate gyrus also exhibits high expression of Hopx during mouse development (Muhlfriedel et al., 2005).

As a corollary of the latNcx being evolutionarily younger than the medNcx, one may expect that as gyrification increases among mammals, it does so to a greater extent in the latNcx than in the medNcx. We explored this possibility by determining the gyrification index (GI) separately for the adult latNcx and medNcx of 20 selected species (Fig. S11A). These 20 species were chosen from the two previously identified principal groups of mammals (10 each), i.e. with a GI≤1.5 vs a GI>1.5 (Lewitus et al., 2014) (see legend to Fig. S11B). Remarkably, plotting the ratio of the neocortical GI (nGI) of adult latNcx/medNcx as a function of overall nGI not only corroborated the existence of these two principal groups of mammals (Fig. S11B) but also revealed that, for either group of mammals, the increase in the nGI among species is typically accompanied by an increase in the ratio of lateral nGI/medial nGI (Fig. S11B). This supports the notion that an increase in gyrification during evolution affected the younger latNcx to a greater extent than the older medNcx.

Finally, the present hypothesis that the progenitor features in the developing mouse medNcx may reflect relicts of the presumptive gyrencephalic ancestor to the mouse was supported by the results of analyzing the gene expression of mouse medial bRGCs in comparison with mouse lateral bRGCs and foetal human bRGCs. This revealed not only that mouse medial bRGCs constitute a cortical progenitor population distinct from mouse lateral bRGCs (Fig. 5A, Fig. S4), but demonstrated that mouse medial bRGCs share many features of their gene expression signature with bRGCs from foetal human neocortex (Fig. 5B). In fact, two genes with high levels of mRNA expression in bRGCs isolated from foetal human neocortex, *FABP7* and *PTPRZ1*, also showed high levels of mRNA expression in bRGCs isolated from embryonic mouse medNcx, in line with these two genes having been implicated in neocortex development and evolution (Pollen et al., 2015). As foetal human bRGCs have been implicated in promoting gyrencephaly (Florio and Huttner, 2014; Fernandez et al., 2016), the latter results are consistent with our hypothesis concerning the evolution of the lissencephalic mouse from a gyrencephalic ancestor.

MATERIALS AND METHODS

Mice

C57BL/6J mice were used unless indicated otherwise. *Tubb3*-GFP transgenic mice (Attardo et al., 2008) were used for bRGC isolation by FACS (see below). Mice were maintained in pathogen-free conditions at the animal facility of the Max Planck Institute of Molecular Cell Biology and Genetics (MPI-CBG), Dresden, Germany. All experiments were performed in accordance with German animal welfare legislation and were overseen by the Institutional Animal Welfare Officer. Necessary licenses were obtained from the regional Ethical Commission for Animal Experimentation of Dresden, Germany (Tierversuchskommission, Landesdirektion Dresden).

Human tissue

Human foetal brain cryosections were from the samples described previously (GW15, corresponding to 13 weeks post-conception)

Development (2018) 145, dev169276. doi:10.1242/dev.169276

(Florio et al., 2015). Human foetal brain tissue was obtained from the Klinik und Poliklinik für Frauenheilkunde und Geburtshilfe, Universitätsklinikum Carl Gustav Carus of the Technische Universität Dresden, following elective pregnancy termination and informed written maternal consents, and with approval of the local University Hospital Ethical Review Committees.

Ferret tissue

Ferret embryonic brain cryosections were from the E36 samples described previously (Turrero Garcia et al., 2016). All experiments were performed in accordance with German animal welfare legislation and were overseen by the Institutional Animal Welfare Officer. Necessary licenses were obtained from the regional Ethical Commission for Animal Experimentation of Dresden, Germany (Tierversuchskommission, Landesdirektion Dresden).

EdU labeling *in vivo*

For *in vivo* EdU labeling, female mice carrying E18.5 embryos were injected intraperitoneally with 100 µl of 1 mg/ml EdU (Sigma) in PBS, or mouse pups at P0 were injected intraperitoneally with 25-30 µl of 1 mg/ml EdU (Sigma) in PBS. Pups were perfused 11 days after EdU injection and processed as described below.

Disruption of Hopx expression and forced Hopx expression

For disruption of Hopx expression and forced Hopx expression, *in utero* electroporation was carried out essentially as described previously (Namba et al., 2014). Briefly, pregnant mice carrying E15.5 embryos were anesthetised using isofluorane. We made use of CRISPR/Cas9-mediated disruption of gene expression in mouse embryonic neocortex (Chen et al., 2015; Kalebic et al., 2016; Shinmyo et al., 2016) and established such disruption for Hopx expression. To achieve this, embryos were injected intraventricularly either with pD1321-AP-gLacZ (Kalebic et al., 2016) (2 µg/µl) (control condition) or with a mixture of pD1321-AP-gHopx #10 (CAGACGCGCACGGACCATGT, 1 µg/µl) plus pD1321-AP-gHopx #13 (GACCCGCCTCGGCTGCGATG, 1 µg/µl) (disruption) in 154 mM NaCl containing 0.1% Fast Green (Sigma) using a glass micropipette, followed by electroporation (27 V, five 50 ms pulses with 950 msec intervals). For forced Hopx expression, embryos were injected either with pCAGGS-empty (control, 1 µg/µl) or with pCAGGS-mHopx (1 µg/µl) together with pCAGGS-EGFP (0.3 µg/µl), followed by electroporation. Electroporated brains were dissected either at E18.5 or at P1 and immersed in 4% paraformaldehyde (PFA) in 120 mM phosphate buffer (pH 7.4) at room temperature followed by fixation for 20-30 h at 4°C.

Analysis of specificity and efficiency of *Hopx* gene disruption

gRNAs targeting the *Hopx* gene were designed, and their efficiency to direct Cas9-mediated cutting of a *Hopx* PCR product was examined, using the methods described previously (Kalebic et al., 2016).

Predicted potential off-target sites of the *Hopx*-targeting gRNAs were identified using Crispor (crispor.tefor.net/), with genome releases GRCm38/mm10 from UCSC Dec.2011 and GCA_001632555.1 C57Bl/6NJ from NCBI as inputs. The same web-tool was used to generate the primer pairs to amplify the off-target amplicons of ∼150 bp using the Primer3 algorithm. We included all off-targets with a cutting frequency determination (CFD) score higher than 0.03 in our analysis. The off-target sites, the CFD off-target scores, chromosomal locations and primer sequences are provided in Table S1.

For analyzing potential off-target effects upon CRISPR/Cas9-mediated disruption of *Hopx* gene expression, brains electroporated as described above were dissected at E18.5, followed by preparation of single-cell suspensions and isolation of PaprikaRFP-positive cells by FACS (10,000 cells per condition) as described below. DNA was isolated from the FACS-isolated cells by standard methods.

Amplicons of on-target and off-target sites were generated by PCR (1 ng DNA from the FACS-isolated cells per PCR) and subjected to Illumina sequencing. Reads were checked for their overall quality using FastQC (v0.11.2). Adapter read trimming was performed with Trimmomatic (v0.36), and paired-end data were merged using FLASH (v1.2.11) and mapped against amplicons with LAST. Amplicons with a coverage of at least 1000 reads were analyzed for non-homologous end joining (NHEJ) events using CRISPResso. For this analysis, only regions complementary to the designed gRNAs plus 25 bp flanking regions were considered.

We assessed the efficiency of the *Hopx* gene disruption with regard to deleting the entire DNA sequence between the gRNA #10 and gRNA #13 target sites as follows. Amplicons containing both target sites and the sequence in between (if still present) were generated by PCR using the DNA from the FACS-isolated cells upon control electroporation and *Hopx* gene disruption. These amplicons were then examined for their size by agarose gel electrophoresis, and the intensity of the bands observed was measured by Fiji. The intensity values were corrected for the length of the respective amplicon.

Isolation of bRGCs from mouse E18.5 medNcx

bRGCs were isolated from E18.5 medNcx of heterozygous *Tubb3*-GFP mouse embryos (pool of two litters) using a previously published method (Florio et al., 2015) with minor modifications. Briefly, the medNcx was subjected to DiI labeling from the basal (pial) side followed by incubation for 3 h at 37°C in an atmosphere of 95% O_2/5% CO_2. We then prepared a single-cell suspension, performed prominin 1 cell-surface staining, isolated DiI^+GFP^-prominin 1^- cells (10,000) by FACS, and lysed the cells followed by storage at −80°C, as described previously (Florio et al., 2015).

Population-level RNA-seq

Total RNA was isolated from the DiI^+GFP^-prominin 1^- cells, a cDNA library was prepared, and cDNA subjected to Illumina sequencing, as described previously (Florio et al., 2015).

Population-level transcriptome data analysis

Sequencing reads obtained from the mouse E18.5 medNcx-derived DiI^+GFP^-prominin 1^- cells were checked for their overall quality using FastQC (v0.11.2). Alignments against the mouse genome reference assembly GRCm38 and quantification of genes of the Ensembl release v81 were carried out using STAR (v2.5.2b). For quality control, duplicated reads were tagged using Picard MarkDuplicates (v2.10.2) and analyzed with dupRadar (v1.8.0). Fastq files of the transcriptomes of mouse E14.5 latNcx-derived and GW15 human neocortex-derived cell populations published previously (Florio et al., 2015) were obtained from the European Nucleotide Archive (Accession Number SRP052294). Alignments and abundance estimation were performed with STAR (v2.5.2b) using Ensembl v81 as reference for mouse samples and Ensembl v88 for human samples. One-to-one orthologs between human and mouse (Ensembl v90) were used to combine the raw counts. Differential gene expression analysis of the combined data was performed with DESeq2 (v1.18.1) using an adjusted *P*-value cutoff of 0.01. Clustering of samples based on rlog normalized counts was visualized using principal component analysis and pheatmap (v1.0.8).

Single-cell RNA-seq and data analysis

Mouse E18.5 medNcx from ∼5 mice was microdissected and pooled to generate a single-cell suspension using the MACS Neural Tissue Dissociation kit according to the manufacturer's instructions. Briefly, the tissue was digested with papain (Miltenyi Biotec, Enzyme Mix 1, 1 ml) for 15 min at 37°C on a rotating wheel, followed by addition of papain inhibitor (Enzyme Mix 2, 15 µl). Tissue was dissociated using 10 gentle triturations (1 ml pipette tip) to obtain a single-cell suspension. Cells were collected by centrifugation at 300 ***g*** for 5 min and resuspended in 600 µl of ice-cold PBS. Cell viability was assessed by Trypan Blue staining, determined using an automatic cell counter (Countess, Thermo Fisher Scientific) and found to amount to 90-95%.

Single cells were captured on a medium (10-17 µm cell diameter) microfluidic chip for mRNA-seq using the Fluidigm C1 system. Cells were loaded onto the chip at a concentration of 400-500 cells/µl and imaged by phase contrast to assess the number of cells per capture site. cDNAs were prepared on chip using the SMARTer v4 Ultra Low RNA kit (Clontech). Size distribution and concentration of single-cell cDNA was assessed by high-throughput capillary gel electrophoresis (Fragment analyzer,

Development (2018) 145, dev169276. doi:10.1242/dev.169276

Advanced Analytical). Sequencing libraries were constructed in 96-well plates using the Illumina Nextera XT DNA Sample Preparation kit using set A and set B primers according to the protocol supplied by Fluidigm. Libraries were quantified by the Agilent Bioanalyzer using the High Sensitivity DNA analysis kit, as well as fluorometrically using the Qubit dsDNA HS Assay kits and a Qubit 2.0 fluorometer (Invitrogen).

Single-cell libraries were pooled, and each cell was sequenced using 100 bp paired-end reads on an Illumina HiSeq 2500 to a depth of greater than 1 million reads. Base calling, adaptor trimming and de-multiplexing was performed as described (Renaud et al., 2013, 2015). Reads were aligned to a Bowtie2 (Langmead and Salzberg, 2012)-indexed mouse genome (mm10 sourced from UCSC) using TopHat (Trapnell et al., 2009) with default settings. Transcript levels were quantified as transcripts per million (TPM), which were converted from fragments per kilobase of mapped reads (FPKM) generated by Cufflinks (Trapnell et al., 2010). We excluded cells with fewer than 1000 expressed genes.

Transcript levels were converted to the log-space by taking the Log_2 TPM. R studio (www.rstudio.com/) was used to run R scripts to perform a principal component analysis (PCA, FactoMineR package) and hierarchical clustering (stats package), and to construct heatmaps, scatter plots and dendrograms. Software packages ggplot2 and gplots were used to generate data graphs. The Seurat package (Macosko et al., 2015) implemented in R was used to identify cell clusters and perform differential gene expression between the clusters. Specifically, we used the FindClusters command (default settings, resolution=0.7) that identifies clusters using a KNN graph based on Euclidean distance in the PCA space, refines edges based on Jacard Similarity and uses the Louvain algorithm to generate the final cell clusters. Cells were defined as Hopx positive when Log_2 TPM was over 5.

Ferret microarray data analysis

The previously published microarray dataset of P2 ferret neocortical zones (De Juan Romero et al., 2015) (GSE60687) were used to analyze the gene expression levels of the ferret orthologs of the previously identified human bRGC-enriched genes (Pollen et al., 2015). Of the latter 64 genes, 58 were found in the ferret dataset. For each of these 58 ortholog genes, the prospective gyrus/prospective sulcus ratio of the expression level in the OSVZ was calculated per probe and per replicate. Subsequently, for each gene, the ratio obtained for all probes and all replicates was averaged.

Immunohistochemistry

Dissected embryonic mouse brain tissue was fixed with 4% PFA in 120 mM phosphate buffer (pH 7.4) for 30 min at room temperature, followed by overnight incubation at 4°C. For all postnatal stages, mouse pups were perfused transcardially with 10-15 ml of 4% PFA in 120 mM phosphate buffer (pH 7.4) at room temperature, followed by post-fixation for 20-30 h at 4°C. Fixed samples were incubated overnight at 4°C in 30% (wt/vol) sucrose in PBS, embedded in Tissue-TEK (OCT, Sakura Finetek) and stored at −20°C. Coronal cryosections (14 µm) and vibratome sections (70 µm) containing rostral or caudal neocortex were cut for immunohistochemistry.

For immunofluorescence, antigen retrieval was performed by incubating the sections, on the glass slide, in 0.01 M sodium citrate buffer for 60 min at 70°C, followed by incubation for 20 min at room temperature. Sections were further permeabilized with 0.3% (wt/vol) Triton X-100 in PBS for 30 min and quenched with 2 mM glycine in PBS for 30 min, followed by blocking with a solution containing 0.2% (wt/vol) gelatin, 300 mM NaCl and 0.3% (wt/vol) Triton X-100 in PBS (blocking buffer). Primary antibodies were diluted in blocking buffer and sections incubated with primary antibodies overnight at 4°C, except for the Hopx antibodies where sections were incubated for 2 days.

The following primary antibodies were used: Pax6 (PRB-278P, Covance, 1:200), Tbr2 (ab15894, Millipore, 1:500), pVim (ab22651, Abcam, 1:400), Sox2 (sc-17320, Santa Cruz, 1:200), Hopx (sc-30216 and sc-398703, Santa Cruz, 1:50), GFP (ab13970, Abcam, 1:1000; MPI-CBG, 1:1000), RFP (ab233, Evrogen, 1:1000), PCNA (CBL407, Millipore, 1:200), Olig2 (MABN50, Millipore, 1:200), S100β (ab868, Abcam, 1:50), NeuN (MAB377, Millipore, 1:50), PH3 (ab10543, Abcam, 1:500) and Satb2 (ab51502, Abcam, 1:200). Incubation with primary antibodies was followed by a 1 h incubation at room temperature with the appropriate A488-, A594-, A555- or A647-labeled (Alexa series, Invitrogen, 1:1000) or Cy2- or Cy3-labeled (Jackson Laboratories, 1:200) secondary goat or donkey antibodies.

EdU was detected using the Click-It kit (Molecular Probes) according to the manufacturer's instructions.

All sections were counterstained with DAPI (Sigma, 1:500) during the secondary antibody incubation and mounted in Mowiol (Merck Biosciences).

Image acquisition and quantification

Fluorescence images were acquired using a Zeiss LSM700 confocal microscope using 10× and 40× objectives. Images were taken as either 8.4 µm (10×) or 1.2 µm (40×) single optical sections. Images taken as tile scans were stitched together using the ZEN software (Zeiss). The VZ was identified as a densely packed $Pax6^+$ or $Sox2^+$ cell layer lining the ventricle. The SVZ or ISVZ were identified as a densely packed $Tbr2^+$ cell layer that is basally adjacent to the VZ. The OSVZ was defined as a zone that contains scattered $Pax6^+$, $Sox2^+$ or $Tbr2^+$ cells. In the case of mouse lateral, ferret and human developing neocortex, the IZ was identified as a zone that is located in between the SVZ (in mouse) or OSVZ (in ferret and human) and the CP, identified as a densely packed $DAPI^+$ cell layer. The boundary between the OSVZ and IZ of mouse embryonic medNcx could not be determined with certainty, which is why we use the OSVZ/IZ labeling in the images. Quantifications were performed using the ZEN software and Fiji. Any $pVim^+$ cell 30 µm from the apical surface was counted as a basal mitotic cell. Hopx immunoreactivity in RFP^+ cells was measured using Fiji. Briefly, an outline of RFP^+ cells was drawn and then the Hopx signal intensity per pixel was measured. Background signal intensity was measured in RFP^+ cells in the CP. Cells with a Hopx signal intensity per pixel above five arbitrary units after background subtraction were considered as $Hopx^+$ cells.

Calculating neocortical gyrification index (nGI)

Calculation of GI was performed as in previous studies (Zilles et al., 1988; Lewitus et al., 2014). nGI values of 20 different species were calculated using images of Nissl-stained coronal sections from neurosciencelibrary.org/ (for *Macropus fuliginosus*, *Procavia capensis*, *Trichechus manatus latirostris*, *Erinaceus europaeus*, *Felis catus*, *Vulpes vulpes*, *Phoca vitulina*, *Mustela putorius*, *Sus scrofa domesticus*, *Capra hircus domestica*, *Tursiops truncates*, *Aotus trivirgatus*, *Eulemur mongoz*, *Macaca mulatta*, *Pan troglodytes*, *Homo sapiens* and *Hydrochaeris hydrochaeris*), brainmaps.org/ (for *Callithrix jacchus* and *Mus musculus*) and Orsini et al. (Orsini et al., 1977) (for *Galago senegalensis*). We used five sections, equally spaced along the rostral-caudal axis of the brain, for each species. The inner and outer contours of medNcx and latNcx were traced using Fiji.

Statistical analysis

Data were tabulated with Excel (Microsoft) and analysed with Statcel3 (OMS, Japan) and MYSTAT (Systat Software, CA). Statistical tests: for two groups of observations that do not follow a normal distribution, the Mann–Whitney *U*-test was used. For two groups of observations that follow a normal distribution with equal variances, the two-tailed Student's *t*-test was used. For two groups of observations that follow a normal distribution with unequal variances, the two-tailed Welch's *t*-test was used. For normality test, the Shapiro-Wilk normality test was used. For homoscedasticity test, the *F* test was used. No animal or data points were excluded from the analyses, except for the dolphin in the regression analysis (least squares method) shown in Fig. S11. Studentised residual>3 was used to determine that the dolphin is an outlier. In all analyses, the investigators were not blinded to sample identity. Results were interpreted as statistically significant when $P<0.05$.

Acknowledgements

We are grateful to the services and facilities of the MPI-CBG for the outstanding support provided, notably Jussi Helppi and his team from the Animal Facility, Jan Peychl and his team from the Light Microscopy Facility, and Liane Funke of the DNA Sequencing Facility. We thank Andreas Dahl for RNA-seq, Nereo Kalebic for donating pD1321-AP-gLacZ, members of the Huttner laboratory for critical discussion, and Svante Pääbo for support of J.G.C. and B.T.

Competing interests
The authors declare no competing or financial interests.

Author contributions
Conceptualization: S.V., T.N.; Validation: S.V., T.N.; Formal analysis: S.V., J.G.C., L.H., C.E.-O., A.-K.H., S.W., H.B., M.S., B.T., W.B.H., T.N.; Investigation: S.V., J.G.C., L.H., C.E.-O., A.-K.H., S.W., H.B., M.S., B.T., T.N.; Writing - original draft: S.V., W.B.H., T.N.; Writing - review & editing: S.V., J.G.C., L.H., C.E.-O., A.-K.H., S.W., H.B., M.S., B.T., W.B.H., T.N.; Supervision: W.B.H.; Funding acquisition: W.B.H.

Funding
T.N. was supported by a long-term fellowship from the Yamada Science Foundation. W.B.H. was supported by grants from the Deutsche Forschungsgemeinschaft (DFG) (SFB 655, A2), the European Research Council (250197) and ERA-NET NEURON (MicroKin).

Data availability
The datasets used to generate Fig. 5 and Figs S4 and S5 have been deposited in NCBI Gene Expression Omnibus under accession numbers GSE120976 and GSE121008.

Supplementary information
Supplementary information available online at
http://dev.biologists.org/lookup/doi/10.1242/dev.169276.supplemental

References
Arai, Y., Pulvers, J. N., Haffner, C., Schilling, B., Nüsslein, I., Calegari, F. and Huttner, W. B. (2011). Neural stem and progenitor cells shorten S-phase on commitment to neuron production. *Nat. Commun.* **2**, 154.

Attardo, A., Calegari, F., Haubensak, W., Wilsch-Bräuninger, M. and Huttner, W. B. (2008). Live imaging at the onset of cortical neurogenesis reveals differential appearance of the neuronal phenotype in apical versus basal progenitor progeny. *PLoS ONE* **3**, e2388.

Bae, B.-I., Jayaraman, D. and Walsh, C. A. (2015). Genetic changes shaping the human brain. *Dev. Cell* **32**, 423-434.

Betizeau, M., Cortay, V., Patti, D., Pfister, S., Gautier, E., Bellemin-Ménard, A., Afanassieff, M., Huissoud, C., Douglas, R. J., Kennedy, H. et al. (2013). Precursor diversity and complexity of lineage relationships in the outer subventricular zone of the primate. *Neuron* **80**, 442-457.

Borrell, V. and Götz, M. (2014). Role of radial glial cells in cerebral cortex folding. *Curr. Opin Neurobiol.* **27**, 39-46.

Chen, F., Rosiene, J., Che, A., Becker, A. and LoTurco, J. (2015). Tracking and transforming neocortical progenitors by CRISPR/Cas9 gene targeting and piggyBac transposase lineage labeling. *Development* **142**, 3601-3611.

De Juan Romero, C., Bruder, C., Tomasello, U., Sanz-Anquela, J. M. and Borrell, V. (2015). Discrete domains of gene expression in germinal layers distinguish the development of gyrencephaly. *EMBO J.* **34**, 1859-1874.

De Toni, A., Zbinden, M., Epstein, J. A., Ruiz i Altaba, A., Prochiantz, A. and Caille, I. (2008). Regulation of survival in adult hippocampal and glioblastoma stem cell lineages by the homeodomain-only protein HOP. *Neural. Dev.* **3**, 13.

Dehay, C., Kennedy, H. and Kosik, K. S. (2015). The outer subventricular zone and primate-specific cortical complexification. *Neuron* **85**, 683-694.

Englund, C., Fink, A., Lau, C., Pham, D., Daza, R. A., Bulfone, A., Kowalczyk, T. and Hevner, R. F. (2005). Pax6, Tbr2, and Tbr1 are expressed sequentially by radial glia, intermediate progenitor cells, and postmitotic neurons in developing neocortex. *J. Neurosci.* **25**, 247-251.

Fernández, V., Llinares-Benadero, C. and Borrell, V. (2016). Cerebral cortex expansion and folding: what have we learned?. *EMBO J.* **35**, 1021-1044.

Fietz, S. A., Kelava, I., Vogt, J., Wilsch-Bräuninger, M., Stenzel, D., Fish, J. L., Corbeil, D., Riehn, A., Distler, W., Nitsch, R. et al. (2010). OSVZ progenitors of human and ferret neocortex are epithelial-like and expand by integrin signaling. *Nat. Neurosci.* **13**, 690-699.

Fietz, S. A., Lachmann, R., Brandl, H., Kircher, M., Samusik, N., Schroder, R., Lakshmanaperumal, N., Henry, I., Vogt, J., Riehn, A. et al. (2012). Transcriptomes of germinal zones of human and mouse fetal neocortex suggest a role of extracellular matrix in progenitor self-renewal. *Proc. Natl. Acad. Sci. USA* **109**, 11836-11841.

Florio, M. and Huttner, W. B. (2014). Neural progenitors, neurogenesis and the evolution of the neocortex. *Development* **141**, 2182-2194.

Florio, M., Albert, M., Taverna, E., Namba, T., Brandl, H., Lewitus, E., Haffner, C., Sykes, A., Wong, F. K., Peters, J. et al. (2015). Human-specific gene ARHGAP11B promotes basal progenitor amplification and neocortex expansion. *Science* **347**, 1465-1470.

Götz, M. and Huttner, W. B. (2005). The cell biology of neurogenesis. *Nat. Rev. Mol. Cell Biol.* **6**, 777-788.

Götz, M., Stoykova, A. and Gruss, P. (1998). Pax6 controls radial glia differentiation in the cerebral cortex. *Neuron* **21**, 1031-1044.

Hansen, D. V., Lui, J. H., Parker, P. R. L. and Kriegstein, A. R. (2010). Neurogenic radial glia in the outer subventricular zone of human neocortex. *Nature* **464**, 554-561.

Hevner, R. F. (2016). Evolution of the mammalian dentate gyrus. *J. Comp. Neurol.* **524**, 578-594.

Kaas, J. H. (2013). The evolution of brains from early mammals to humans. *Wiley Interdiscip. Rev. Cognit. Sci.* **4**, 33-45.

Kalebic, N., Taverna, E., Tavano, S., Wong, F. K., Suchold, D., Winkler, S., Huttner, W. B. and Sarov, M. (2016). CRISPR/Cas9-induced disruption of gene expression in mouse embryonic brain and single neural stem cells in vivo. *EMBO Rep.* **17**, 338-348.

Kelava, I., Lewitus, E. and Huttner, W. B. (2013). The secondary loss of gyrencephaly as an example of evolutionary phenotypical reversal. *Front. Neuroanat.* **7**, 16.

Langmead, B. and Salzberg, S. L. (2012). Fast gapped-read alignment with Bowtie 2. *Nat. Methods* **9**, 357-359.

Lein, E. S., Belgard, T. G., Hawrylycz, M. and Molnár, Z. (2017). Transcriptomic perspectives on neocortical structure, development, evolution, and disease. *Annu. Rev. Neurosci.* **40**, 629-652.

Lewitus, E., Kelava, I., Kalinka, A. T., Tomancak, P. and Huttner, W. B. (2014). An adaptive threshold in mammalian neocortical evolution. *PLoS Biol.* **12**, e1002000.

Li, D., Takeda, N., Jain, R., Manderfield, L. J., Liu, F., Li, L., Anderson, S. A. and Epstein, J. A. (2015). Hopx distinguishes hippocampal from lateral ventricle neural stem cells. *Stem Cell Res.* **15**, 522-529.

Lodato, S. and Arlotta, P. (2015). Generating neuronal diversity in the mammalian cerebral cortex. *Annu. Rev. Cell Dev. Biol.* **31**, 699-720.

Lui, J. H., Hansen, D. V. and Kriegstein, A. R. (2011). Development and evolution of the human neocortex. *Cell* **146**, 18-36.

Macosko, E. Z., Basu, A., Satija, R., Nemesh, J., Shekhar, K., Goldman, M., Tirosh, I., Bialas, A. R., Kamitaki, N., Martersteck, E. M. et al. (2015). Highly parallel genome-wide expression profiling of individual cells using nanoliter droplets. *Cell* **161**, 1202-1214.

Mariotto, A., Pavlova, O., Park, H.-S., Huber, M. and Hohl, D. (2016). HOPX: The unusual homeodomain-containing protein. *J. Invest. Dermatol.* **136**, 905-911.

Martínez-Cerdeño, V., Cunningham, C. L., Camacho, J., Antczak, J. L., Prakash, A. N., Cziep, M. E., Walker, A. I. and Noctor, S. C. (2012). Comparative analysis of the subventricular zone in rat, ferret and macaque: evidence for an outer subventricular zone in rodents. *PLoS ONE* **7**, e30178.

Martínez-Martínez, M. A., De Juan Romero, C., Fernández, V., Cárdenas, A., Götz, M. and Borrell, V. (2016). A restricted period for formation of outer subventricular zone defined by Cdh1 and Trnp1 levels. *Nat. Commun.* **7**, 11812.

Mitchell, C. and Silver, D. L. (2018). Enhancing our brains: Genomic mechanisms underlying cortical evolution. *Semin. Cell Dev. Biol.* **76**, 23-32.

Mühlfriedel, S., Kirsch, F., Gruss, P., Stoykova, A. and Chowdhury, K. (2005). A roof plate-dependent enhancer controls the expression of Homeodomain only protein in the developing cerebral cortex. *Dev. Biol.* **283**, 522-534.

Mühlfriedel, S., Kirsch, F., Gruss, P., Chowdhury, K. and Stoykova, A. (2007). Novel genes differentially expressed in cortical regions during late neurogenesis. *Eur. J. Neurosci.* **26**, 33-50.

Namba, T. and Huttner, W. B. (2017). Neural progenitor cells and their role in the development and evolutionary expansion of the neocortex. *Wiley Interdiscip. Rev. Dev. Biol.* **6**, e256.

Namba, T., Kibe, Y., Funahashi, Y., Nakamuta, S., Takano, T., Ueno, T., Shimada, A., Kozawa, S., Okamoto, M., Shimoda, Y. et al. (2014). Pioneering axons regulate neuronal polarization in the developing cerebral cortex. *Neuron* **81**, 814-829.

Nowakowski, T. J., Pollen, A. A., Sandoval-Espinosa, C. and Kriegstein, A. R. (2016). Transformation of the radial glia scaffold demarcates two stages of human cerebral cortex development. *Neuron* **91**, 1219-1227.

O'Leary, M. A., Bloch, J. I., Flynn, J. J., Gaudin, T. J., Giallombardo, A., Giannini, N. P., Goldberg, S. L., Kraatz, B. P., Luo, Z.-X., Meng, J. et al. (2013). The placental mammal ancestor and the post-K-Pg radiation of placentals. *Science* **339**, 662-667.

Ono, K., Takebayashi, H. and Ikenaka, K. (2009). Olig2 transcription factor in the developing and injured forebrain; cell lineage and glial development. *Mol. Cells* **27**, 397-401.

Orsini, J. G., Christolomme, A., Dupe-Godet, M. and Riche, D. (1977). Stereotaxic brain atlas of the prosimian primate galago senegalensis. *Mammalia* **41**, 445-515.

Osumi, N., Shinohara, H., Numayama-Tsuruta, K. and Maekawa, M. (2008). Concise review: Pax6 transcription factor contributes to both embryonic and adult neurogenesis as a multifunctional regulator. *Stem Cells* **26**, 1663-1672.

Pollen, A. A., Nowakowski, T. J., Chen, J., Retallack, H., Sandoval-Espinosa, C., Nicholas, C. R., Shuga, J., Liu, S. J., Oldham, M. C., Diaz, A. et al. (2015). Molecular Identity of Human Outer Radial Glia during Cortical Development. *Cell* **163**, 55-67.

Rakic, P. (2009). Evolution of the neocortex: a perspective from developmental biology. *Nat. Rev. Neurosci.* **10**, 724-735.

Reillo, I., de Juan Romero, C., García-Cabezas, M. A. and Borrell, V. (2011). A role for intermediate radial glia in the tangential expansion of the mammalian cerebral cortex. *Cereb. Cortex* **21**, 1674-1694.
Renaud, G., Kircher, M., Stenzel, U. and Kelso, J. (2013). freelbis: an efficient basecaller with calibrated quality scores for Illumina sequencers. *Bioinformatics* **29**, 1208-1209.
Renaud, G., Stenzel, U., Maricic, T., Wiebe, V. and Kelso, J. (2015). deML: robust demultiplexing of Illumina sequences using a likelihood-based approach. *Bioinformatics* **31**, 770-772.
Sanides, F. (1969). Comparative architectonics of the neocortex of mammals and their evolutionary interpretation. *Ann. N Y Acad. Sci.* **167**, 404-423.
Shinmyo, Y., Tanaka, S., Tsunoda, S., Hosomichi, K., Tajima, A. and Kawasaki, H. (2016). CRISPR/Cas9-mediated gene knockout in the mouse brain using in utero electroporation. *Sci. Rep.* **6**, 20611.
Shitamukai, A., Konno, D. and Matsuzaki, F. (2011). Oblique radial glial divisions in the developing mouse neocortex induce self-renewing progenitors outside the germinal zone that resemble primate outer subventricular zone progenitors. *J. Neurosci.* **31**, 3683-3695.
Smart, I. H. M., Dehay, C., Giroud, P., Berland, M. and Kennedy, H. (2002). Unique morphological features of the proliferative zones and postmitotic compartments of the neural epithelium giving rise to striate and extrastriate cortex in the monkey. *Cereb. Cortex* **12**, 37-53.
Sousa, A. M. M., Meyer, K. A., Santpere, G., Gulden, F. O. and Sestan, N. (2017). Evolution of the Human Nervous System Function, Structure, and Development. *Cell* **170**, 226-247.
Stahl, R., Walcher, T., De Juan Romero, C., Pilz, G. A., Cappello, S., Irmler, M., Sanz-Aquela, J. M., Beckers, J., Blum, R., Borrell, V. et al. (2013). Trnp1 regulates expansion and folding of the Mammalian cerebral cortex by control of radial glial fate. *Cell* **153**, 535-549.
Striedter, G. F., Srinivasan, S. and Monuki, E. S. (2015). Cortical folding: when, where, how, and why?. *Annu. Rev. Neurosci.* **38**, 291-307.
Sun, T. and Hevner, R. F. (2014). Growth and folding of the mammalian cerebral cortex: from molecules to malformations. *Nat. Rev. Neurosci.* **15**, 217-232.
Taverna, E., Götz, M. and Huttner, W. B. (2014). The cell biology of neurogenesis: toward an understanding of the development and evolution of the neocortex. *Annu. Rev. Cell Dev. Biol.* **30**, 465-502.
Thomsen, E. R., Mich, J. K., Yao, Z., Hodge, R. D., Doyle, A. M., Jang, S., Shehata, S. I., Nelson, A. M., Shapovalova, N. V., Levi, B. P. et al. (2016). Fixed single-cell transcriptomic characterization of human radial glial diversity. *Nat. Methods* **13**, 87-93.
Trapnell, C., Pachter, L. and Salzberg, S. L. (2009). TopHat: discovering splice junctions with RNA-Seq. *Bioinformatics* **25**, 1105-1111.
Trapnell, C., Williams, B. A., Pertea, G., Mortazavi, A., Kwan, G., van Baren, M. J., Salzberg, S. L., Wold, B. J. and Pachter, L. (2010). Transcript assembly and quantification by RNA-Seq reveals unannotated transcripts and isoform switching during cell differentiation. *Nat. Biotechnol.* **28**, 511-515.
Turrero García, M., Chang, Y. J., Arai, Y. and Huttner, W. B. (2016). S-phase duration is the main target of cell cycle regulation in neural progenitors of developing ferret neocortex. *J. Comp. Neurol.* **524**, 456-470.
Wang, X., Tsai, J.-W., LaMonica, B. and Kriegstein, A. R. (2011). A new subtype of progenitor cell in the mouse embryonic neocortex. *Nat. Neurosci.* **14**, 555-561.
Wang, L., Hou, S. and Han, Y.-G. (2016). Hedgehog signaling promotes basal progenitor expansion and the growth and folding of the neocortex. *Nat. Neurosci.* **19**, 888-896.
Wong, F. K., Fei, J.-F., Mora-Bermúdez, F., Taverna, E., Haffner, C., Fu, J., Anastassiadis, K., Stewart, A. F. and Huttner, W. B. (2015). Sustained Pax6 expression generates primate-like basal radial glia in developing mouse neocortex. *PLoS Biol.* **13**, e1002217.
Zilles, K., Armstrong, E., Schleicher, A. and Kretschmann, H.-J. (1988). The human pattern of gyrification in the cerebral cortex. *Anat. Embryol.* **179**, 173-179.

Vaid et al., Fig. S1

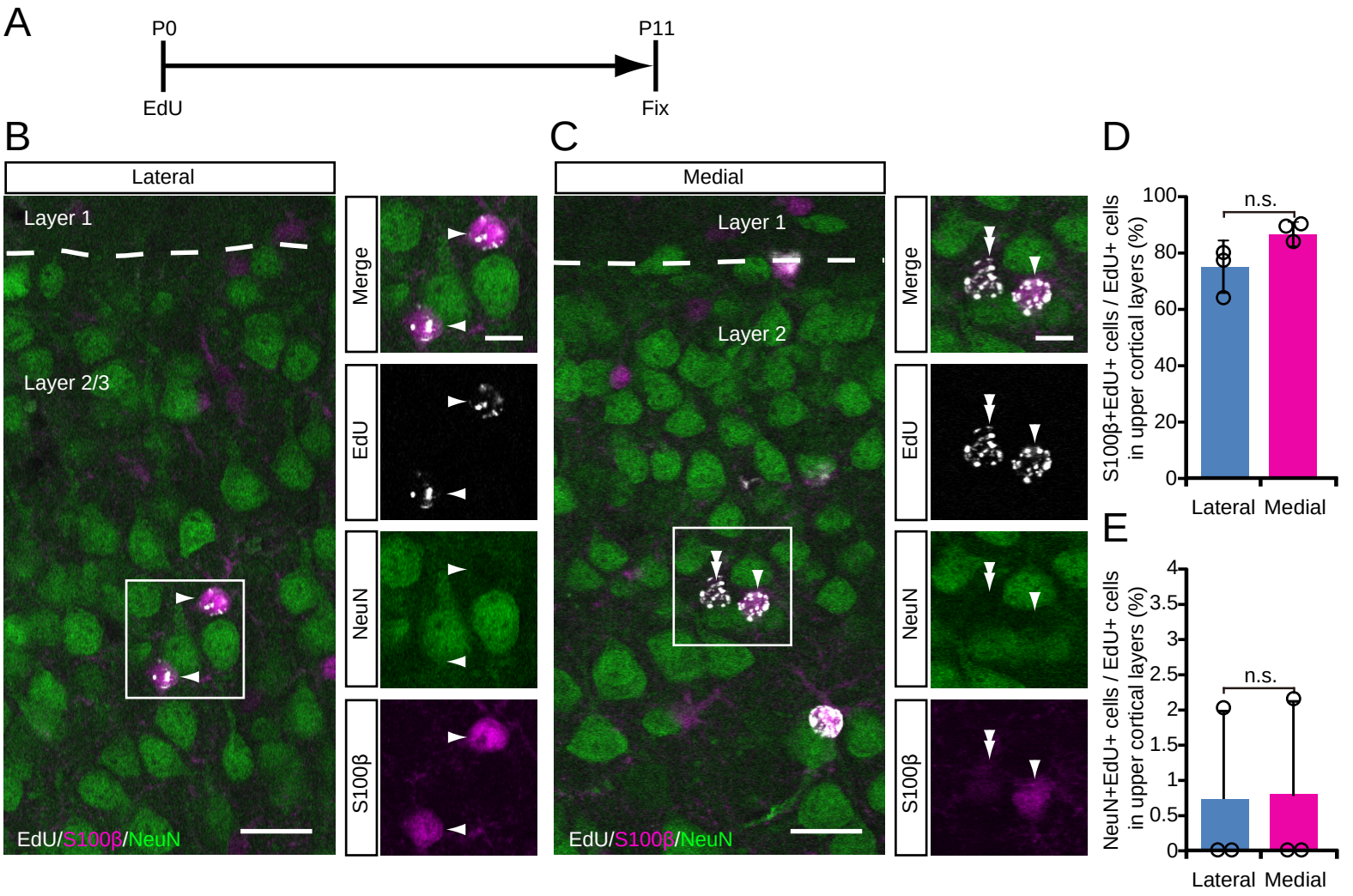

Figure S1. Progenitor cells in mouse P0 latNcx and medNcx give rise mostly to astrocytes.

Mice were labeled by an EdU pulse at P0 and analyzed at P11 (see **A**).

(**B**,**C**) EdU (white), NeuN (green) and S100β (magenta) triple immunofluorescence of cortical layers 2 and 3 (area within 200 µm from boundary between layer 1 and 2 (dashed lines)) of P11 lateral (**B**) and medial (**C**) neocortex. White boxes indicate the areas shown at higher magnification in the respective right panels. Single arrowheads indicate NeuN–S100β+EdU+ cells, and double arrowheads NeuN–S100β–EdU+ cells.

(**D**) Quantification of the percentage of EdU+ cells in the lateral (blue) and medial (magenta) upper cortical layers that are S100β+. Note that most of the EdU+ cells analyzed at P11 following an EdU pulse at P0 expressed the astroglial marker S100ß, indicating that they were the progeny of gliogenic progenitors.

(**E**) Quantification of the percentage of EdU+ cells in the lateral (blue) and medial (magenta) upper cortical layers that are NeuN+. Note that hardly any NeuN+ EdU+ neurons were detected at P11 following an EdU pulse at P0.

(**D**,**E**) Error bars indicate SD; n.s., not statistically significant; Welch's *t*-test in **D** (n = 3 mice, $P = 0.15$, $\varphi = 2.78$, $t = -1.96$), and Mann–Whitney U-test in **e** (n = 3 mice, $P = 0.32$). Open circles in the bar graphs in **D** and **E** represent individual data points.

(**B**,**C**) Images are single 0.4-µm optical sections; scale bars, 20 µm (left panels in **B**,**C**) and 10 µm (right panels in **B**,**C**).

Vaid et al., Fig. S2

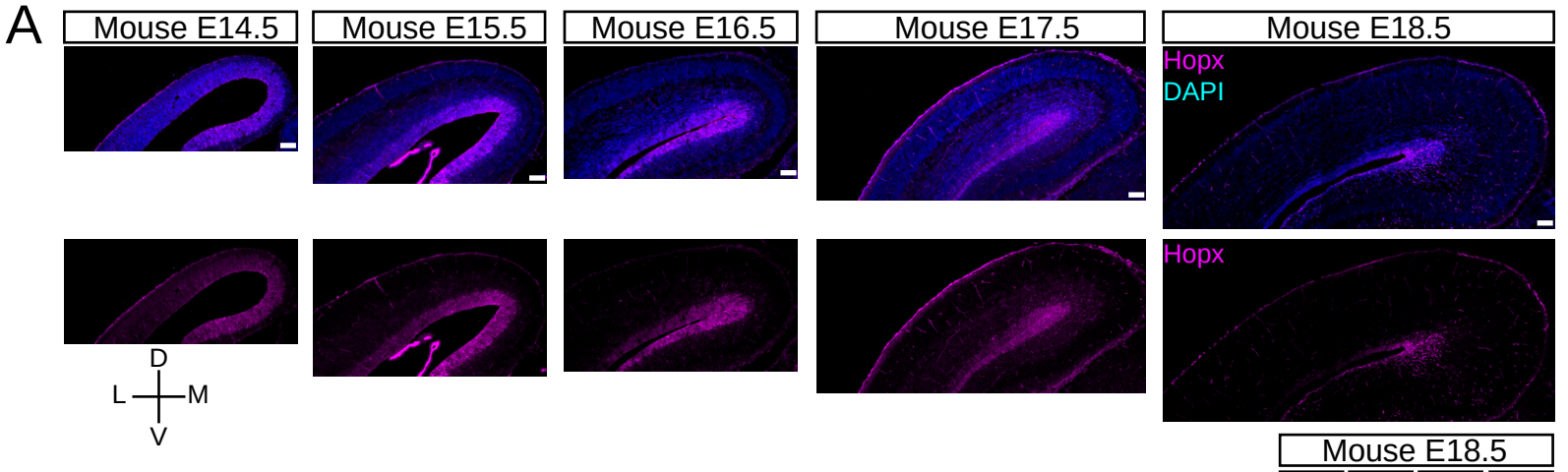

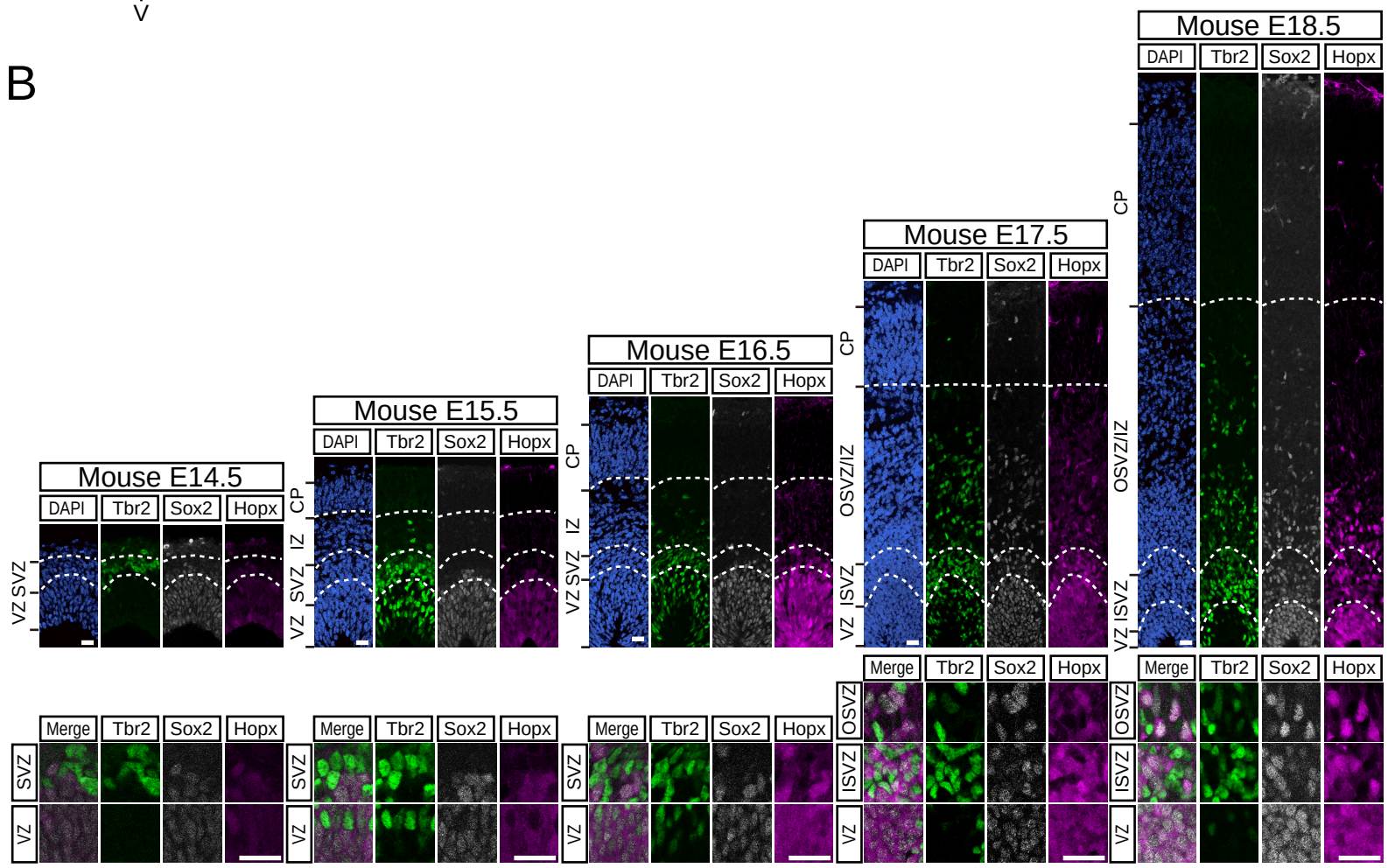

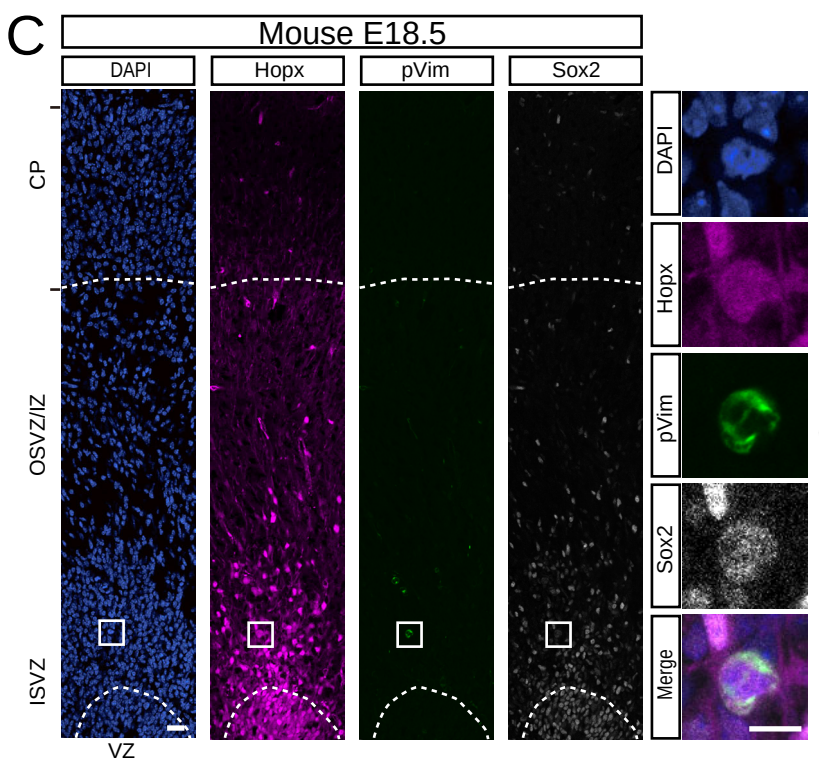

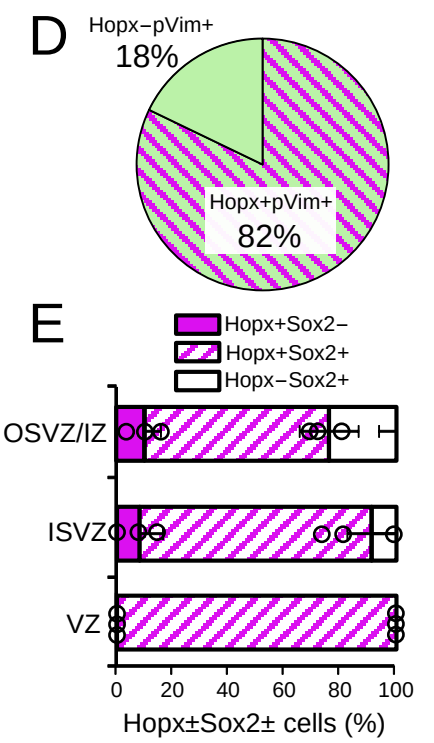

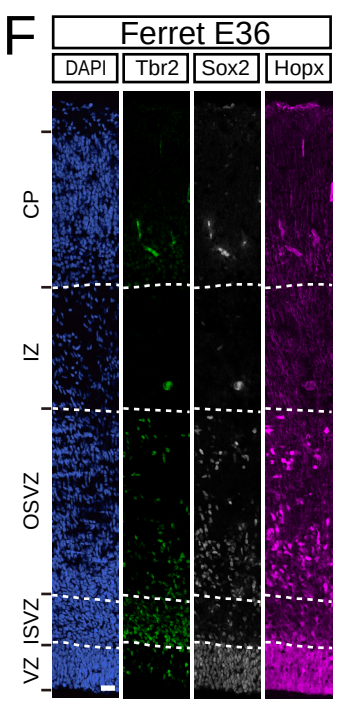

Figure S2. Pattern of Hopx expression in the embryonic mouse and ferret neocortex.

(**A**) Hopx immunofluorescence (magenta), combined with DAPI staining (blue), in the mouse neocortex at E14.5, E15.5, E16.5, E17.5 and E18.5. D, dorsal; M, medial; V, ventral; L, lateral.

(**B**) Hopx (magenta), Sox2 (white) and Tbr2 (green) triple immunofluorescence, combined with DAPI staining (blue), in the mouse medNcx at E14.5, E15.5, E16.5, E17.5 and E18.5. Dashed lines indicate the boundaries between VZ, SVZ, IZ, ISVZ, OSVZ/IZ and CP. Lower panels show higher-magnification images of VZ, SVZ, ISVZ and OSVZ.

(**A,B**) Note that Hopx immunoreactivity in the latNcx was detected at a low level in the VZ at E14.5 but decreased with the progression of neocortical development and eventually disappeared by E18.5. In contrast, in the medNcx, which was immunostained for Sox2 and Tbr2 to distinguish VZ, ISVZ and OSVZ, Hopx immunoreactivity in the VZ increased from E14.5 until E18.5 and became detectable in the ISVZ and OSVZ at E17.5. Note further that these dynamics of Hopx expression in developing mouse medNcx are similar to what has been reported for fetal human neocortex, where during early gestation (GW13.5) Hopx+ cells are present mainly in the VZ, whereas later in gestation (GW14.5) Hopx+ cells are present also in the ISVZ and OSVZ(Pollen et al., 2015).

(**C**) Hopx (magenta), pVim (green) and Sox2 (white) triple immunofluorescence, combined with DAPI staining (blue), in the mouse E18.5 medNcx. White boxes in the

left panels indicate the areas shown at higher magnification in the right panels. Dashed lines indicate the boundaries between VZ, ISVZ-OSVZ/IZ, and CP.

(**D**) Quantification of the percentage of basal pVim+ cells that are Hopx+ (green with diagonal magenta lines) and Hopx– (green only) in the mouse E18.5 medNcx.

(**E**) Quantification of the percentage of cells that express Hopx and/or Sox2 in the indicated zones of the mouse E18.5 medNcx; Hopx+Sox2– (solid magenta), Hopx+Sox2+ (diagonal magenta lines) and Hopx–Sox2+ (solid white). Error bars indicate SD. Open circles in the bar graph represent individual data points (n = 3 embryos); note that the sum of the three cell populations was set to 100% for each of the three embryos.

(**F**) Hopx (magenta), Sox2 (white) and Tbr2 (green) triple immunofluorescence, combined with DAPI staining (blue), in the ferret E36 latNcx. Dashed lines indicate the boundaries between VZ, ISVZ, OSVZ, IZ and CP.

(**A**,**B**,**C**,**F**) Images in **A** are single 4.3-µm optical sections, images in **B**,**C** and **F** are single 0.6-µm optical sections; scale bars, 100 µm (**A**), 20 µm (**B** and left panels in **C**), 10 µm (right panels in **c**), and 50 µm (**F**).

Vaid et al., Fig. S3

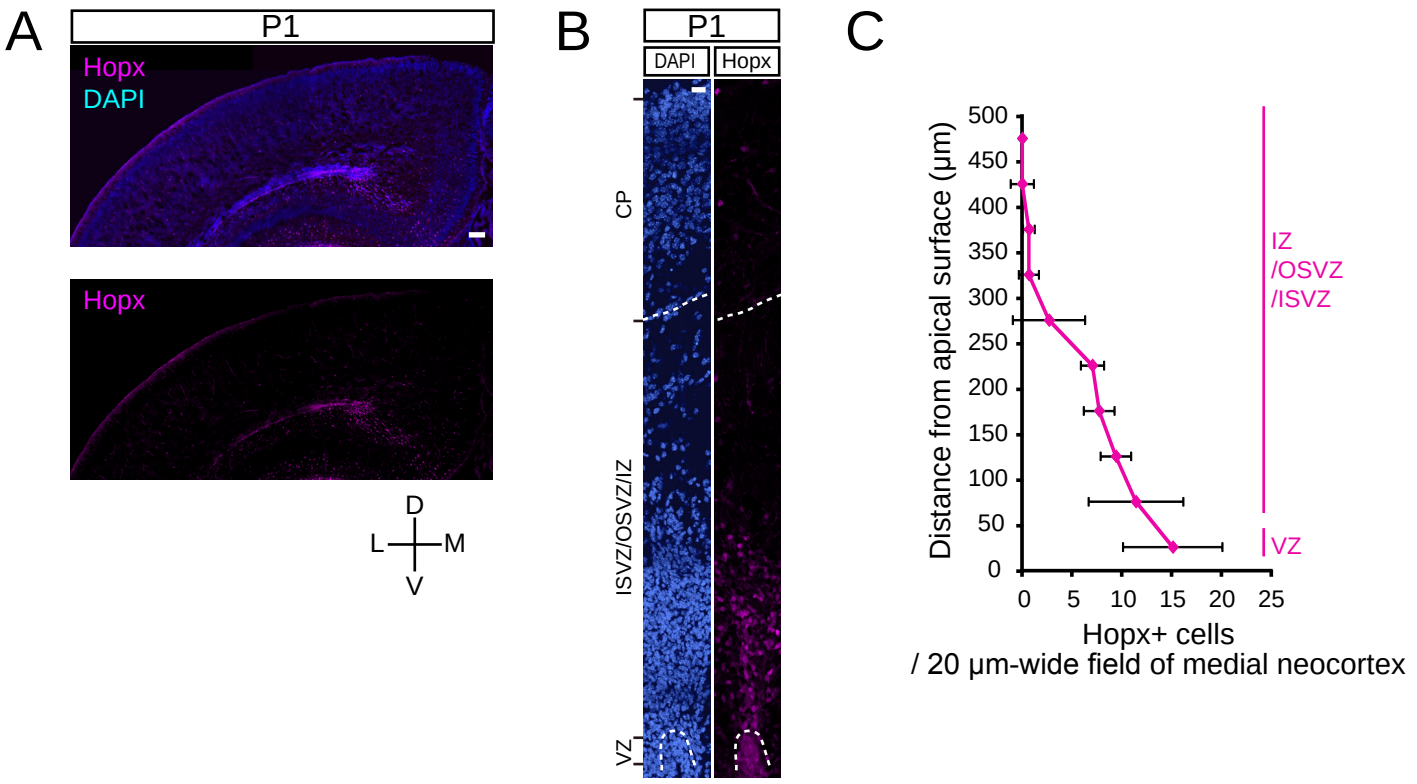

Figure S3. Expression of Hopx in the early postnatal mouse neocortex.

(**A**) Hopx immunofluorescence (magenta), combined with DAPI staining (blue), in the mouse neocortex at P1. D, dorsal; M, medial; V, ventral; L, lateral.

(**B**) Hopx (magenta) immunofluorescence, combined with DAPI staining (blue), in the mouse medNcx at P1. Dashed lines indicate the boundaries between VZ, ISVZ/OSVZ/IZ and CP.

(**C**) Quantification of the distribution of Hopx+ cells along a 500-µm radial axis (divided into 10 bins) of the medNcx (20 µm-wide field) at P1. Error bars indicate SD.

(**A**,**B**) Images in **A** are 17-µm merged stacks (7 partly overlapping single 4.3-µm optical sections), images in **B** are single 0.6-µm optical sections; scale bars, 50 µm (**A**) and 20 µm (**B**).

Vaid et al., Fig. S 4

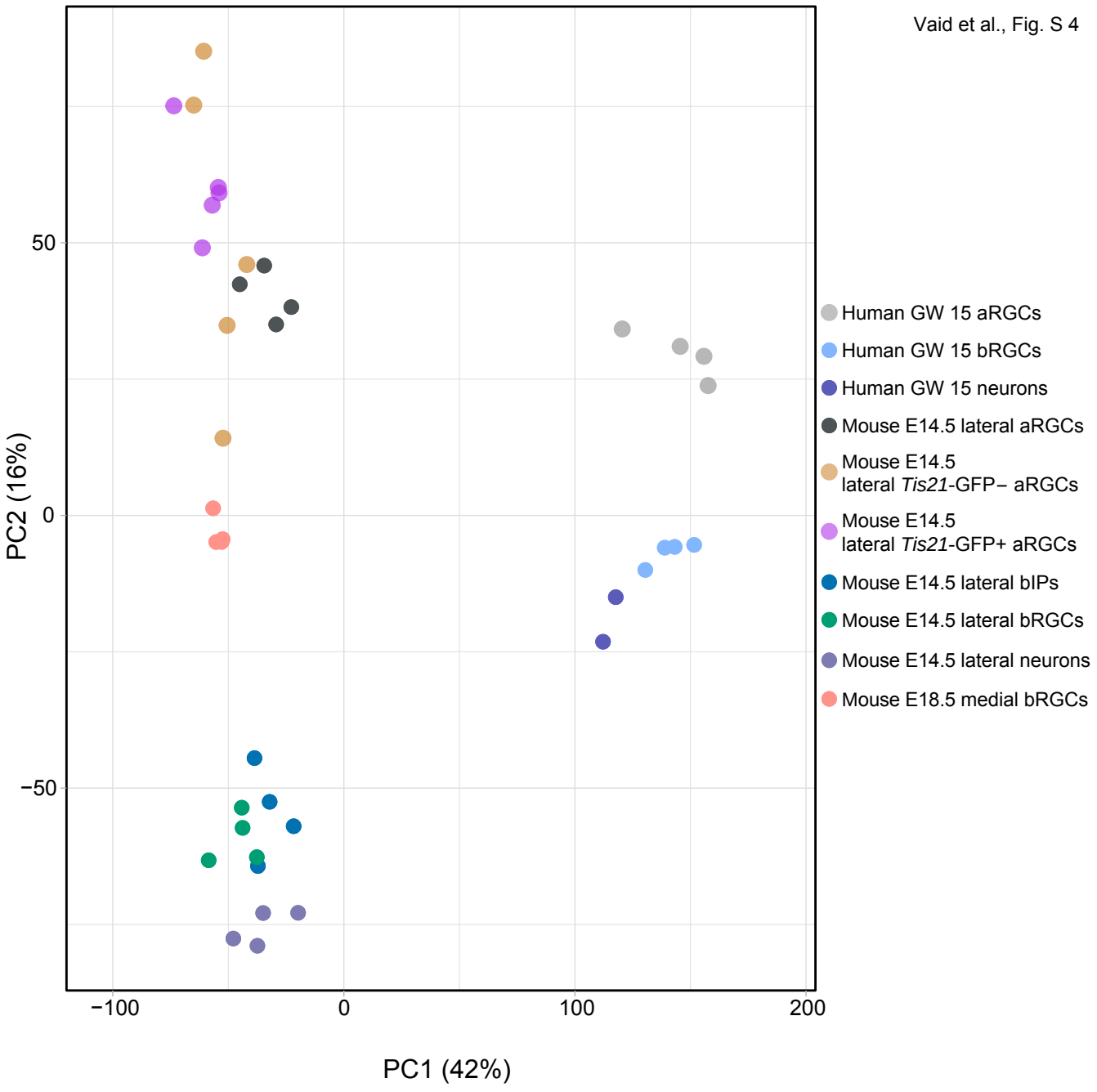

Figure S4. PCA of RNAseq data obtained from various isolated mouse and human cortical progenitor cell populations and neurons.

PCA of RNA-seq data of (i) bRGCs isolated from mouse E18.5 medNcx (this study), (ii) cortical progenitor populations isolated from mouse E14.5 latNcx (Florio et al., 2015) (GSE65000), and (iii) bRGCs isolated from human GW15 neocortex (Florio et al., 2015) (GSE65000), as indicated by the various colored dots (4-5 replicates per cell population). The percentages of variance explained by PC1 and PC2 are indicated. Note that the greatest difference between these cortical cell populations was between mouse and human cell populations, as revealed by PC1, and that the next greatest difference was between human aRGCs vs. human bRGCs and neurons, and between mouse lateral aRGCs, *Tis21*-GFP– negative and –positive aRGCs vs. mouse medial bRGCs vs. mouse lateral bRGCs, bIPs and neurons, as revealed by PC2.

Vaid et al., Fig. S5

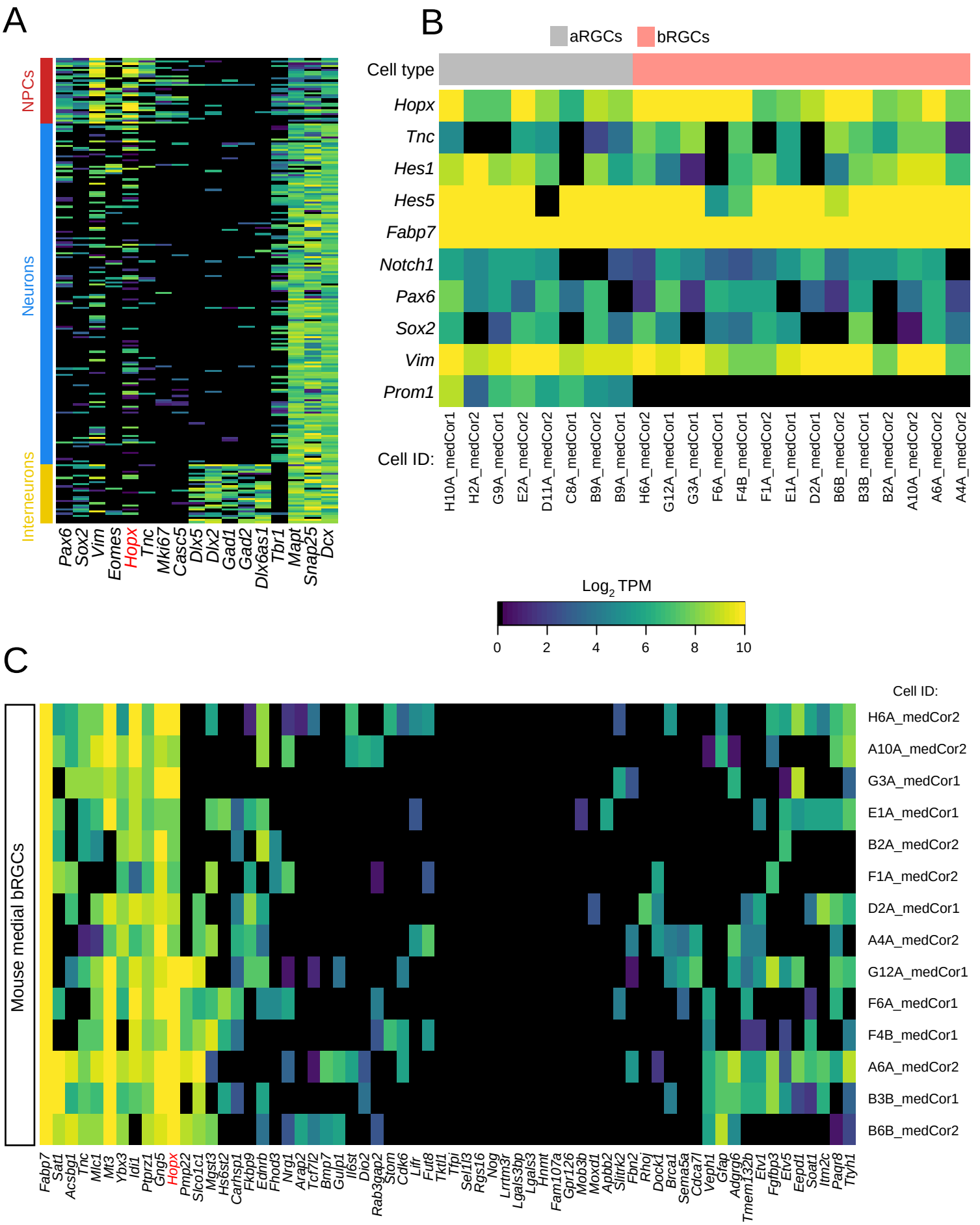

Figure S5. Single-cell RNA-seq of cells isolated from mouse E18.5 medNcx.

Single-cell RNA-seq analysis on 221 disscociated cells obtained from microdissected mouse E18.5 medNcx (two independent analyses using a pool of 8 neocortices each).

(**A**) Heatmap of expression of selected genes expression in individual cells. PCA was used to identify cell populations. Cells are in rows, genes in columns. Color codes for cell populations: NPCs (31 neocortical progenitor cells, red), excitatory cortical neurons (162 cells, blue), interneurons (28 cells, yellow).

(**B**) Heatmap of selected radial glia marker gene expression in the 22 neocortical progenitor cells that express *Hopx* >5 in Log_2 TPM. aRGCs (grey, 8 cells) and bRGCs (red, 14 cells) are separated based on the absence (black) or presence (colors) of *Prom1* expression. Cells are in columns, marker genes in rows.

(**C**) Heatmap showing the expression of the 64 mouse orthologs of the human bRGC-enriched genes (Pollen et al., 2015) in the 14 bRGCs identified in (**B**). Cells are in rows, genes in columns. Note that essentially all of these cells showed detectable expression of most, if not all, of these 64 genes.

(**B**,**C**) The last number of the cell ID indicates from which of the two independent experiments the cell originated.

Vaid et al., Fig. S6

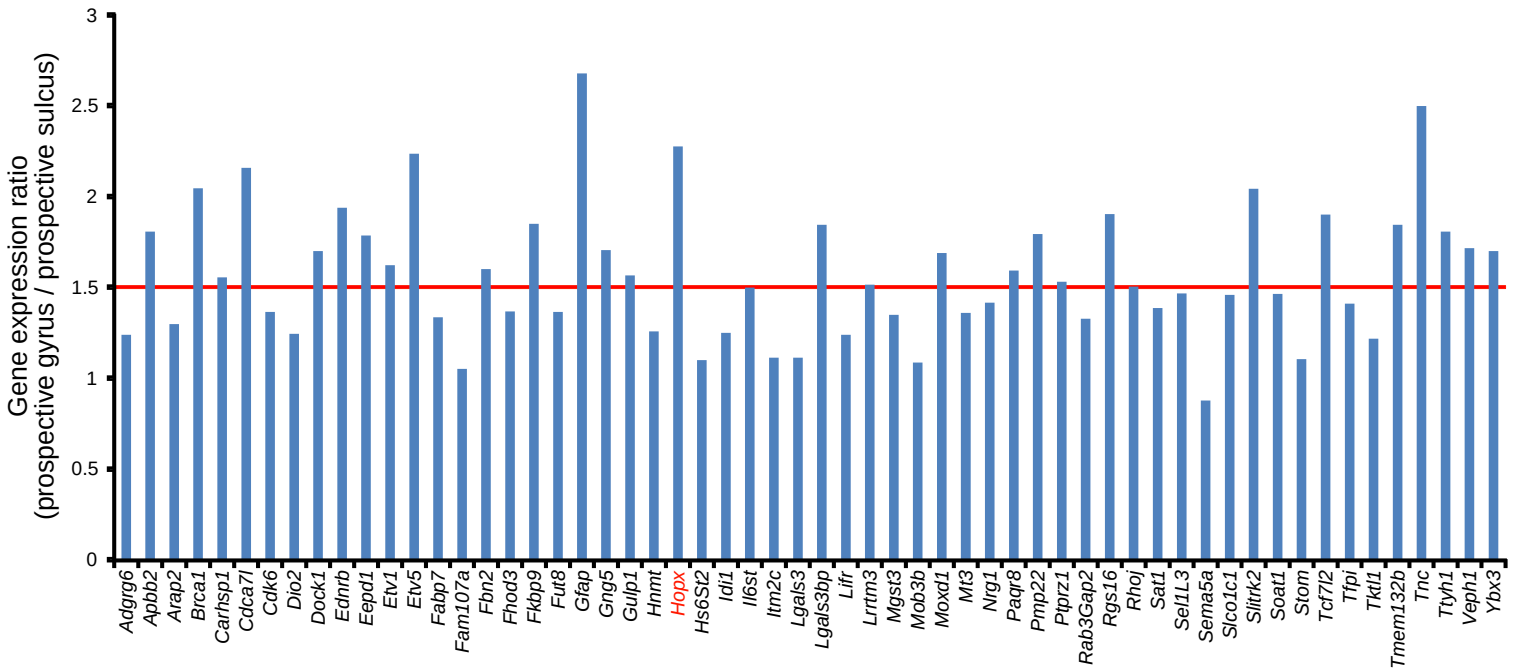

Figure S6. Expression of human bRGC-enriched genes in the OSVZ of developing ferret neocortex.

Gene expression levels of 58 of the 64 human bRGC-enriched genes (Pollen et al., 2015) in the P2 ferret OSVZ are expressed as prospective gyrus / prospective sulcus ratio. Microarray data are from a previous publication (De Juan Romero et al., 2015) (GSE60687). Red line indicates a ratio of gene expression levels of 1.5. Note that 30 genes show an at least 1.5-fold greater expression level in the OSVZ of the prospective gyrus than the OSVZ of the prospective sulcus.

Vaid et al., Fig. S7

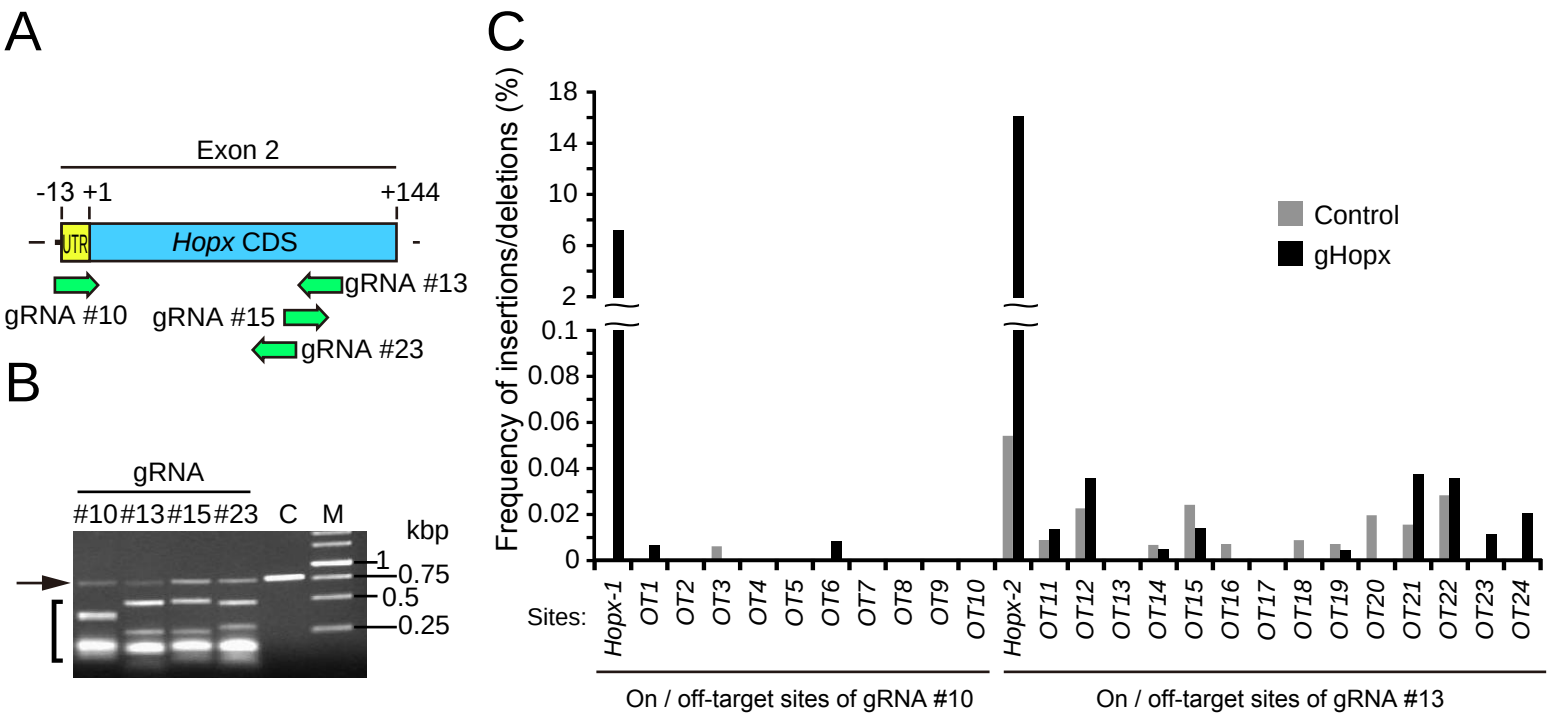

Figure S7. CRISPR/Cas9-mediated disruption of Hopx expression in the embryonic mouse medNcx and its effect on the level of mitotic BPs.

We established CRISPR/Cas9-mediated disruption of Hopx expression in mouse embryonic neocortex, using a mixture of two guide RNAs (gRNA #10 + gRNA #13) (see panels A-E). An analysis of the distribution of the intensity of Hopx immunoreactivity in these cells between control and gHopx electroporation allowed us to identify a threshold level above and below which cells were defined as Hopx+ and Hopx–, respectively (see Methods and panel F).

(**A,B**) Schematic diagram of exon 2 (157 nt) of the *Hopx* gene indicating the target positions of four gRNAs (**A**), and their efficiency to direct on-target cutting of a genomic 750-bp *Hopx* PCR product by Cas9 in vitro, as revealed by agarose gel electrophoresis (**B**). Arrow, uncut *Hopx* PCR product; bracket, fragments of cut *Hopx* PCR product. C, *Hopx* PCR product-only control with no gRNA added; M, DNA size markers as indicated on the right. Note the effectiveness of gRNA #10 and gRNA #13.

(**C-E**) In vivo specificity. Analysis of on- and off-target sites in PaprikaRFP-expressing cells isolated by FACS at E18.5 from mouse medNcx electroporated at E15.5 with either a plasmid encoding Cas9_T2A_PaprikaRFP and a gRNA targeting LacZ (control, ctrl; Kalebic et al., 2016), or with a mixture of two plasmids, each encoding Cas9_T2A_PaprikaRFP and one of the two gRNAs targeting Hopx (gHopx, either gRNA #10 or gRNA #13). Three embryos each were electroporated for control and gHopx, and the cells isolated from each set of embryos were pooled for analyses. (**C**) DNA sequencing analysis of amplicons containing either the *Hopx* site (*Hopx-1*) and 10 off-target sites (*OT1-10*) of gRNA #10 (~24,000 reads), or the *Hopx* site (*Hopx-2*) and 14 off-target sites (*OT11-24*) of gRNA #13 (~32,000 reads). Data are expressed as percentage of insertions and deletions at the *Hopx* sites and the respective predicted off-target sites as compared to the mouse genome reference sequence over the number

of aligned reads. Note that the frequency of mismatches at the predicted off-target sites upon gHopx electroporation was very low (<0.04%) and in the same range as the occurrence of mismatches at the two *Hopx* target sites upon control electroporation (<0.05% of ~50,000 reads). (**D**) Agarose gel electrophoresis of an amplicon containing both *Hopx* sites of gRNA#10 and gRNA #13. Arrow and arrowhead, *Hopx* PCR product without and with the deletion of the DNA sequence between the two *Hopx* target sites, respectively. Note the loss of the DNA between the two target sites in about 40% of cases (**E**) Quantification of the *Hopx* PCR product bands shown in **D**, expressed as a length-corrected intensity ratio of the lower band (with the ≈100 bp deletion) to the upper band (without the ≈100 bp deletion).

(**F**-**I**) Mouse E15.5 medNcx was *in utero* electroporated with either a plasmid encoding Cas9_T2A_PaprikaRFP and a gRNA targeting LacZ (control, Ctrl), or with a mixture of two plasmids, each encoding Cas9_T2A_PaprikaRFP and one of the two gRNAs targeting Hopx (gHopx, either gRNA #10 or gRNA #13), all under constitutive promoters, followed by analysis at E18.5. (**F**) Quantification of Hopx immunoreactivity in RFP+ cells in the VZ. (**G**,**H**) RFP (magenta) and PH3 (white) double immunofluorescence, combined with DAPI staining (blue), upon control (**G**) and gHopx (**H**) electroporation. White boxes in the left panels indicate the areas shown at higher magnification in the respective right panels. Arrows indicate basal RFP+ cells in mitosis, as revealed by PH3 immunofluorescence. Dashed lines indicate the boundary between ventricle and VZ. Images in left panels are 5-µm merged stacks (15 partly overlapping single 0.6-µm optical sections), images in right panels are single 0.6-µm optical sections; scale bars, 50 µm (left panels) and 10 µm (right panels). (**I**) Quantification of the percentage of RFP+ cells in the SVZ that are PH3+ upon control (grey column) and gHopx (black column) electroporation.

(**E**,**F**,**I**) Error bars indicate SD; *, *P* <0.05; Student's *t*-test in **F** (n = 3 embryos, *P* = 0.0.011, φ = 4, t = 4.50), Mann-Whitney's U test in **I** (n = 3 embryos, *P* = 0.0495). Open circles in the bar graphs represent individual data points.

Vaid et al., Fig. S8

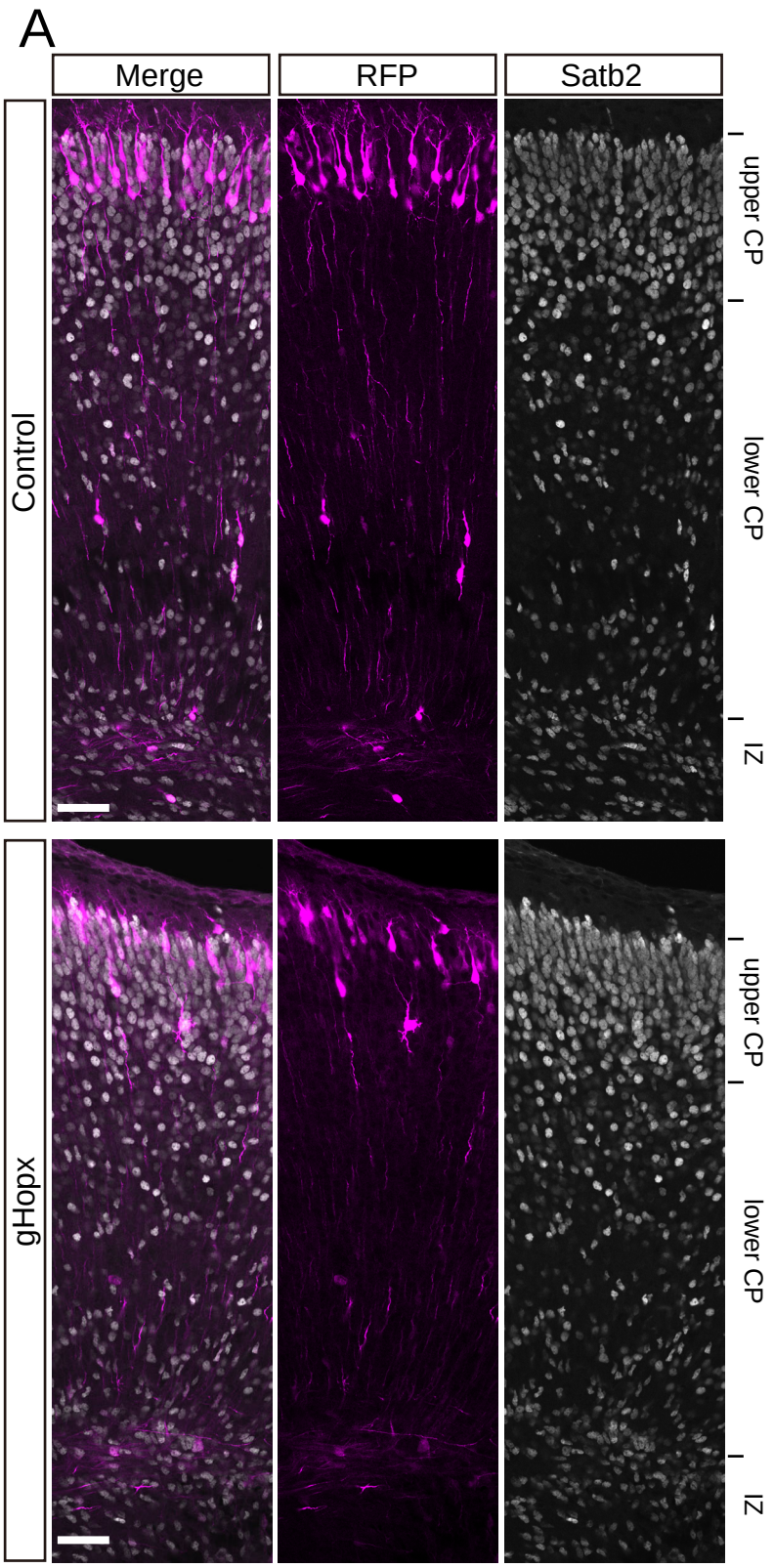

Figure S8. Effect of CRISPR/Cas9-mediated disruption of Hopx expression on neurogenesis in the early postnatal mouse neocortex.

We quantified the proportion of Satb2+ neurons among the progeny of the targeted cells (PaprikaRFP+) at P1. This analysis showed that disruption of Hopx expression in the embryonic mouse medNcx resulted in a significant, ~40% decrease in the proportion of the Satb2+ neurons that were still migrating to the CP upper layers, among the progeny of the targeted cells.

For this analysis, mouse E15.5 medNcx was *in utero* electroporated with either a plasmid encoding Cas9_T2A_PaprikaRFP and a gRNA targeting LacZ (control, Ctrl), or with a mixture of two plasmids, each encoding Cas9_T2A_PaprikaRFP and one of the two gRNAs targeting Hopx (gHopx, either gRNA #10 or gRNA #13), all under constitutive promoters, followed by analysis at P1.

(**A**) RFP (magenta) and Satb2 (white) double immunofluorescence, upon control (top) and gHopx (bottom) electroporation. Images are single 0.6-µm optical sections; scale bars, 50 µm.

(**B**) Quantification of the percentage of RFP+ cells in the wall of the medNcx (50 µm-wide microscopic field) that express Satb2, a marker of late-born neurons (Britanova et al., 2008; Molyneaux et al., 2015), and located in the lower CP, IZ and SVZ, i.e. newborn Satb2+ neurons that were still migrating to the CP upper layers at P1, upon control (grey column) and gHopx (black column) electroporation. Error bars indicate SD; *, P <0.05. Student's t-test (n = 5 (control) and 4 (gHopx) embryos, P = 0.0.04994, φ = 7, t = 2.37). Open circles represent individual data points.

Vaid et al., Fig. S9

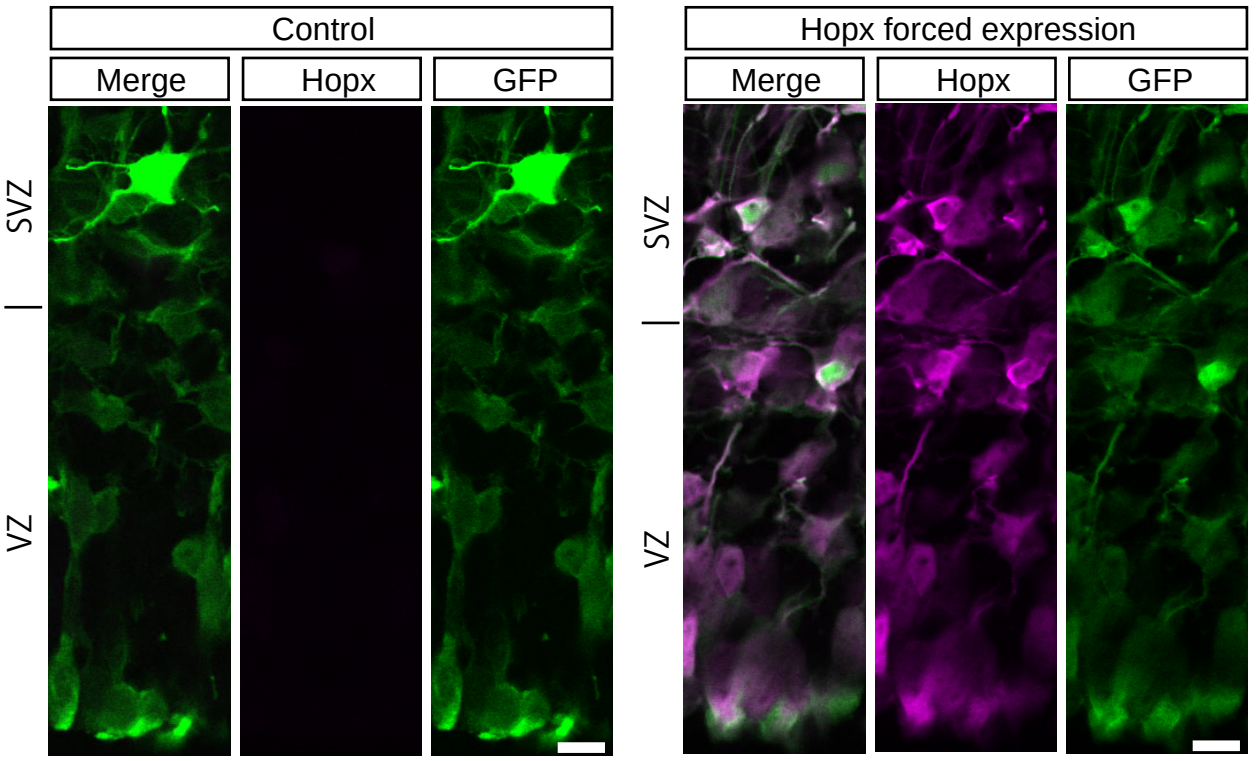

Figure S9. Presence of Hopx protein in the progeny of the electroporated cells upon forced Hopx expression in the embryonic mouse latNcx.

Mouse E15.5 latNcx was *in utero* co-electroporated with a plasmid encoding GFP together with either an empty vector (control) or a Hopx expression plasmid (Hopx forced expression), all under constitutive promoters, followed by analysis at E18.5. GFP (green) and Hopx (magenta) double immunofluorescence upon control (left) and Hopx forced expression (right). Images are 5-µm merged stacks (15 partly overlapping single 0.6-µm optical sections); scale bars, 10 µm.

Vaid et al., Fig. S10

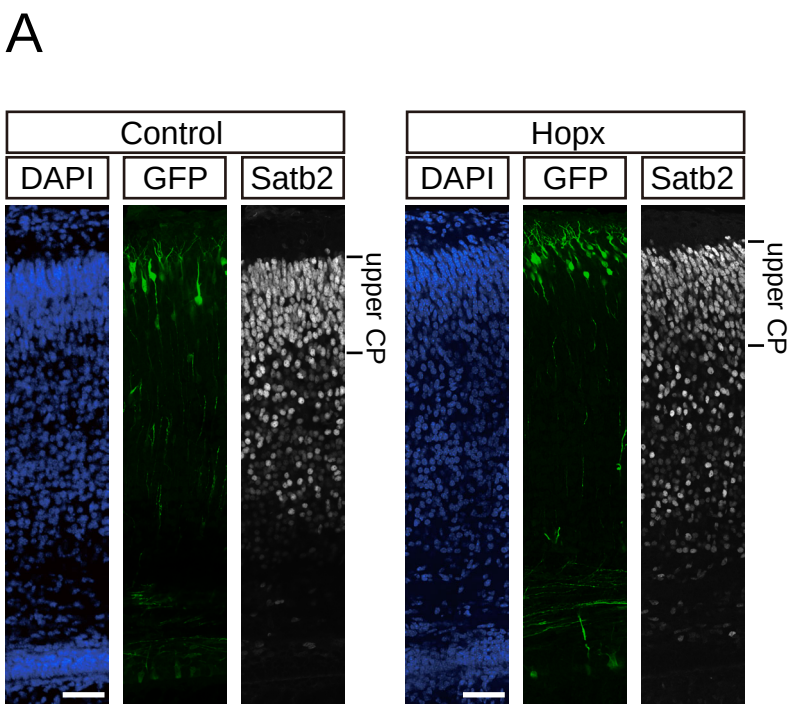

Figure S10. Effect of forced Hopx expression on neurogenesis in the early postnatal mouse neocortex.

We quantified the proportion of Satb2+ neurons among the progeny of the targeted cells (GFP+) at P1. This analysis showed that forced Hopx expression in the embryonic mouse latNcx initiated at E15.5 resulted in a significant, ~40% increase in the proportion of Satb2+ neurons that had arrived in the upper cortical layers, among the progeny of the targeted cells in the upper CP at P1.

For this analysis, mouse E15.5 latNcx was *in utero* co-electroporated with a plasmid encoding GFP together with either an empty vector (control, Ctrl) or a Hopx expression plasmid (Hopx), all under constitutive promoters, followed by analysis at P1.

(**A**) GFP (green) and Satb2 (white) double immunofluorescence, combined with DAPI staining (blue), upon control (left) and Hopx (right) electroporation. Images are single 0.6-µm optical sections; scale bars, 50 µm. Images are single 0.6-µm optical sections; scale bars, 50 µm.

(**B**) Quantification of the percentage of GFP+ cells in the wall of the latNcx (50 µm-wide microscopic field) that are Satb2+ and located in the upper CP, i.e. Satb2+ neurons that had arrived in the upper cortical layers by P1, upon control electroporation (grey column) and forced Hopx expression (black column). Error bars indicate SD; *, $P < 0.05$. Student's *t*-test (n = 4 embryos, $P = 0.036$, $\varphi = 6$, $t = -2.69$). Open circles represent individual data points.

Vaid et al., Fig. S11

A

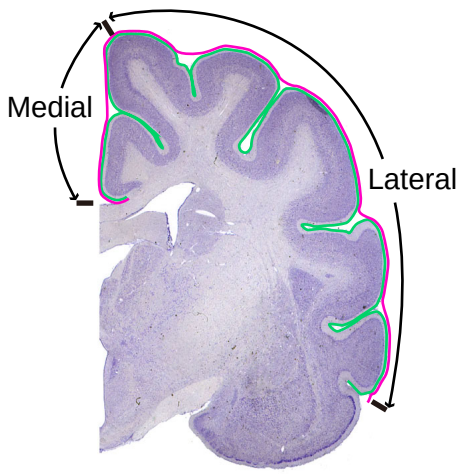

B

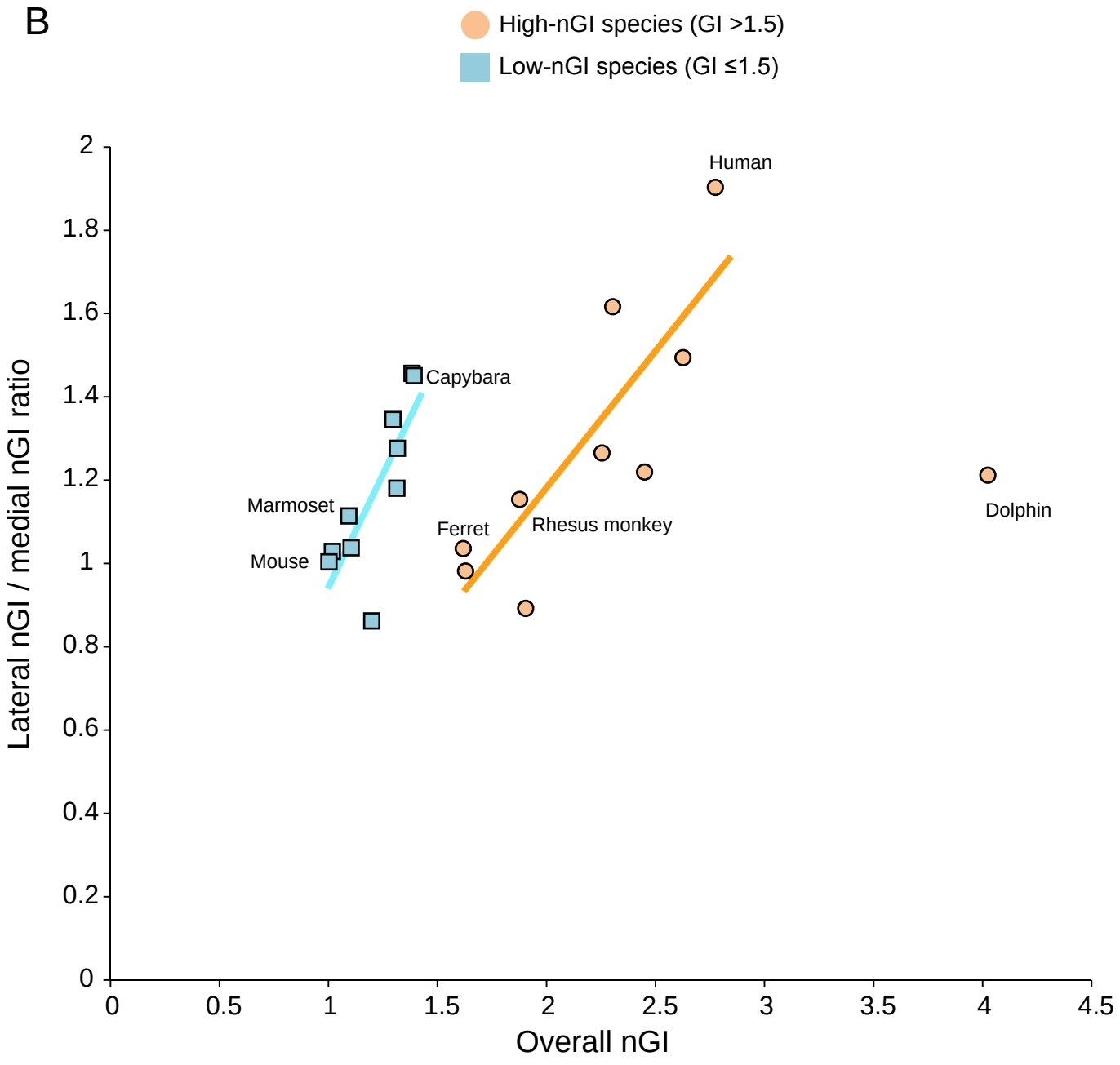

Figure S11. Increase in overall nGI among species is accompanied by an increase in the lateral nGI / medial nGI ratio.

(**A**) Illustration of the determination of the lateral nGI / medial nGI ratio. Coronal section of the neocortex of an adult *Felis catus* (obtained from http://neurosciencelibrary.org/); green line, inner contour; magenta line, outer contour. MedNcx and latNcx are indicated by double-headed arrows.

(**B**) Lateral nGI / medial nGI ratio as a function of overall nGI in the two principal groups of mammals (GI ≤1.5 vs. GI >1.5) (Lewitus et al., 2014). Blue squares, 10 selected low nGI (≤1.5) species (mouse (indicated), hedgehog, marmoset (indicated), manatee, bushbaby, owl monkey lemur, kangaroo, hyrax, capybara (indicated)); orange circles, 10 selected high nGI (>1.5) species (ferret (indicated), cat, rhesus monkey (indicated), fox, chimpanzee, boar, goat, seal, human (indicated), dolphin (indicated); blue line, regression analysis of the 10 low nGI species, $y = 1.083x - 0.137$, $R^2 = 0.63$, $P = 0.0059$; orange line, regression analysis the 9 high nGI species without the dolphin (studentized residual = 7.56), $y = 0.656x - 0.132$, $R^2 = 0.71$, $P = 0.0043$.

Table S1. Information of on- and off-target sites and probes

Amplicon name	On / off-target sequence	Locus	Chromosome	chromosome location		CFD Score*	primer-forward	primer-reverse
Hopx-1	CAGACGCGCACGGACCATGTCGG	Hopx	chr 5	77094960	77094979	1	AGGATCTCCACCTGGTCCTC	GGCCATCTGGTTCCCCTG
OT-1	CAGTCGTGCACAGACCATGTGGG	intergenic:Ccdc147-Sorcs3	chr19	48157623	48157717	0.48257576	CCATTATCAGGCGAGTGGAGG	CTCACTTTGGGGTAGGGCTG
OT-2	CAGAAACTCACGGACAATGTTGG	intergenic:Ccdc167-Mdga1	chr17	29775843	29775911	0.35714286	CCCTTCCCCGGGTAAGAAAC	GCCCTTCCCCTTTAACAGCT
OT-3	CAGACACCCAAGGACCATCTTGG	intergenic:C230014O12Rik-Pbx3	chr2	34170387	34170497	0.20689655	CAACAGACTGACCCAGGACA	TGAGCTGTGTGGTTTTGCAA
OT-4	CAGACTCTCAAGCACCATGTAGG	intron:9030622O22Rik	chr2	148009234	148009346	0.13157895	GGGGTGCTGGATCCTTTTGA	TCTATACAATGGACTGGGCAGA
OT-5	CAGTCTCACATGGACCATGTTGG	intergenic:Plch1-Gm16162	chr3	63806483	63806590	0.13053613	GAGAAGTAGGAGGCAGGGGA	CCCCTAACCTCACATGGCTC
OT-6	CAGAAGCTCACGGGCCATCTAGG	intergenic:Gm24504-Nedd4l	chr18	64804093	64804199	0.07471264	GGGTGTGTATTGGGTATGTGC	ACAGGAACCAGAGACCGAGA
OT-7	CAGAAGCACAGGGACCATCTAGG	intergenic:Adra2a-Gpam	chr19	54583375	54583463	0.06403941	TGTGAGTGTTCATCTCTGGATGG	TTTTGCTCCTCTCCAACCCC
OT-8	CAGAGGTGCACGGAACATCTGGG	intergenic:Gm26489-1700028P15Rik	chr2	171592476	171592498	0.04856322	CACCAGGCTTGTGGGAGATT	AGCCAGCAGTATGGATCGTG
OT-9	CAGACAGGCATGGACTATGTTGG	intergenic:Gm8349-Arhgef26	chr3	61664889	61664991	0.04455273	TGTGACAGTGCCATTTGAGAGA	CCTCTGGCACACCTACCAAC
OT-10	CAGAGGGGCAGCGACCATGTTGG	exon:Map1a	chr2	121301773	121301903	0.03737024	CAGCCAGTCTGCAGAGAGTG	TGGCTGAGGACACATGTTCC
Hopx-2	GACCCGCCTCGGCTGCGATGAGG	Hopx	chr 5	77094848	77094979	1	ATAGGCTTGGGGACTCACCT	GAGGACCAGGTGGAGATCCT
OT-11	TAACCACCTCAGCTGCGATGAGG	exon:1700026L06Rik	chr2	28693019	28693041	0.86666667	CGCCTCCATAGTGGTTCCTG	CCACCTGCTCACTATCCTGC
OT-12	AAACTGCCCCGGCTGCGATGGGG	exon:Reep6	chr10	80335486	80335508	0.45818182	CCAGATTCCCAGCAAGTCCC	AGAGTCCCACTGGGCAGTC
OT-13	GCCACGCGCCGGCTGCGATGGGG	intergenic:Prkcb-Cacng3	chr7	122649519	122649541	0.39262993	TCCCCTCGTCTATGCCTTCA	TGGGTGGGCATAGCAACAG
OT-14	GAACCACCTCAGCTGCGAAGAGG	intron:Wdfy3	chr5	101883241	101883263	0.24761905	CCCAGCACTAGAGTTCTGGC	ACTGTGGCACTTCTGGCTTT
OT-15	GCTCCGCCTCGGCCGCGATGAGG	intergenic:Fabp5-Gm9833	chr3	10088140	10088162	0.15433673	AAACTTCAAAAGCGTCCGGC	CCTCGGACTTGTCGGCATC
OT-16	GCTCCGCCTCGGCCGCGATGAGG	exon:Myef2	chr2	125123529	125123551	0.15433673	CCTCGGACTTGTCGGCATC	GCTCGGGGCCTTTTCAAATC
OT-17	GACCTGCCTGGGCTGCAGTGTGG	intron:Erg	chr16	95446484	95446612	0.09239057	TGTCAAAGTTGCCCAGACTGT	CCAGTTCCCAGCCTTGAGAC
OT-18	GACTCGTCTCTGCTGTGATGTGG	intergenic:Gm25431-Ighmbp2	chr19	3160762	3160678	0.07692308	CCCATCACAAGGCCCATCAA	TGTAAGGCTGTTTTGCGTGG
OT-19	GTTCGGCCTCGGCTGCGAGGCGG	exon:Smarce1	chr11	99230283	99230305	0.075	CTGTTCCGGACGGGGTTG	GTGGTGTTTCTGCTTGGCG
OT-20	GCCCCGCCGCTTCTGCGATGTGG	intron:Nudt15	chr14	73524725	73524747	0.07195186	CTGACTTAGCTACCCTTCCCC	GGGACTTTTCCTTTTGCCCC
OT-21	GTCCCGCCTCCCCTGCGATCCGG	exon:Decr1	chr4	15945294	15945316	0.0707192	CTGCCTTACCCTCTGAGGAC	TGAGTCCTGCTGCAGACATG
OT-22	GACCCACCTCGGGTGAGTTGGGG	exon:Aplp2	chr9	31161748	31161770	0.06818182	AGCAGGCAACACTAAGAACA	CCGACGCATAGCTCTGGAAA
OT-23	GACCAGGCTGGGCTGCGTTGAGG	intron:Dlg4	chr11	70029326	70029348	0.05228758	CGCCCTGCAGTTTAGCTAGA	AAAGGGTTAAAGCGAGGCGT
OT-24	GACTCACCTCGGCTTCGGTGGGG	intron:Slc6a6	chr6	91697120	91697142	0.04571429	GCCTCACCCGTTGCAGATAT	GAAGTCACTGGGCCTTCCTC
							*Cutting Frequency Determination (CFD) score	

Supplementary references

Britanova, O., de Juan Romero, C., Cheung, A., Kwan, K. Y., Schwark, M., Gyorgy, A., Vogel, T., Akopov, S., Mitkovski, M., Agoston, D. et al. (2008). Satb2 is a postmitotic determinant for upper-layer neuron specification in the neocortex. *Neuron* **57**, 378-392.

De Juan Romero, C., Bruder, C., Tomasello, U., Sanz-Anquela, J. M. and Borrell, V. (2015). Discrete domains of gene expression in germinal layers distinguish the development of gyrencephaly. *EMBO J.* **34**, 1859-1874.

Florio, M., Albert, M., Taverna, E., Namba, T., Brandl, H., Lewitus, E., Haffner, C., Sykes, A., Wong, F. K., Peters, J. et al. (2015). Human-specific gene ARHGAP11B promotes basal progenitor amplification and neocortex expansion. *Science* **347**, 1465-1470.

Lewitus, E., Kelava, I., Kalinka, A. T., Tomancak, P. and Huttner, W. B. (2014). An adaptive threshold in mammalian neocortical evolution. *PLoS Biol.* **12**, e1002000.

Molyneaux, B. J., Goff, L. A., Brettler, A. C., Chen, H. H., Brown, J. R., Hrvatin, S., Rinn, J. L. and Arlotta, P. (2015). DeCoN: genome-wide analysis of in vivo transcriptional dynamics during pyramidal neuron fate selection in neocortex. *Neuron* **85**, 275-288.

Pollen, A. A., Nowakowski, T. J., Chen, J., Retallack, H., Sandoval-Espinosa, C., Nicholas, C. R., Shuga, J., Liu, S. J., Oldham, M. C., Diaz, A. et al. (2015). Molecular Identity of Human Outer Radial Glia during Cortical Development. *Cell* **163**, 55-67.